Highlights

Amount of carbon fixed, transit time and fate of harvested wood products define the climate change mitigation potential of boreal forest management - A model analysis

Holger Metzler, Samuli Launiainen, Giulia Vico

- We combine an ecophysiological growth model with tree allometries from forest inventories
- We evaluate wood production and climate change mitigation potential
- Potential climate change mitigation depends on carbon time away from the atmosphere
- This is affected by management, including mixing species and ages
- Assessing management options requires following carbon in ecosystem and wood products

Amount of carbon fixed, transit time and fate of harvested wood products define the climate change mitigation potential of boreal forest management - A model analysis

Holger Metzler[a,c,*], Samuli Launiainen[b], Giulia Vico[a]

[a] *Department of Crop Production Ecology, Swedish University of Agricultural Sciences (SLU), PO Box 7043, Uppsala, 750 07, Sweden*
[b] *Natural Resources Institute Finland, Latokartanonkaari 9, Helsinki, 00790, Finland*
[c] *Present address: Department of Forest Ecology and Management, Swedish University of Agricultural Sciences (SLU), Skogsmarksgränd 17, Umeå, 901 83, Sweden*

Abstract

Boreal forests are often managed to maximize wood production, but other goals, among which climate change mitigation, are increasingly important. Examining synergies and trade-offs between forest production and its potential for carbon sequestration and climate change mitigation in forest stands requires explicitly accounting for how long forest ecosystems and wood products retain carbon from the atmosphere (i.e., the carbon transit time). We propose a novel mass-balanced process-based compartmental model that allows following the carbon path from its photosynthetical fixation until its return to the atmosphere by autotrophic or heterotrophic respiration, or by being burnt as wood product. We investigate four management scenarios: mixed-aged pine, even-aged pine, even-aged spruce, and even-aged mixed forest. The even-aged clear-cut based scenarios reduced the carbon amount in the system by one third in the first 18 yr. Considering only the amount of carbon stored in the ecosystem, these initial losses are compensated after $42 - 45$ yr. At the end of an 80 yr rotation, the even-aged forests hold up to 31 % more carbon than the the mixed-aged forest. However, mixed-aged

*Corresponding author: holger.metzler@slu.se

forest management is superior to even-aged forest management during almost the entire rotation when factoring in the carbon retention time away from the atmosphere, i.e., in terms of climate change mitigation potential. Importantly, scenarios that maximize production or amount of carbon stored in the ecosystems are not necessarily the most beneficial for carbon retention away from the atmosphere. These results underline the importance of considering carbon transit time when evaluating forest management options for potential climate change mitigation and hence explicitly tracking carbon in the system, e.g. via models like the one developed here.

Keywords: boreal forest management, wood production, carbon sequestration, transit time, climate change mitigation, process-based modelling

---

Statements and Declarations

Competing Interests: The authors have no relevant financial or non-financial interests to disclose.

Code Repository: The Python code to reproduce the figures used in the manuscript is available as a documented package at `https://github.com/goujou/BFCPM`.

In case of publication this repository will be transformed into a permanent repository with DOI.

1. Introduction

Boreal forests are one of the largest biomes on Earth and strongly regulate global climate through land-surface energy, water and carbon cycles (Bonan, 2008, Chapin III et al., 2000, Baldocchi et al., 2000). These forests are in large part managed (Högberg et al., 2021), often to maximize timber production and economic income (Millennium ecosystem assessment, 2005). They comprise approximately 45 % of the global stock of growing timber (Vanhanen

et al., 2012), contributing to the economic well-being and cultural heritage of the Nordic societies (Millennium ecosystem assessment, 2005, Vanhanen et al., 2012) and providing numerous ecosystem services (Maes et al., 2016, Vihervaara et al., 2010). Nevertheless, the focus on production has led to degradation of other important services, among which climate regulation, collectable goods, recreation, water regulation and purification, maintenance of soil productivity and air-quality regulation (Pohjanmies et al., 2017).

There is an increasing commitment to more sustainable forest management and preserving ecosystem services (Larsen et al., 2022, Kellomäki, 2022). There is also an increasing interest in carbon sequestration by boreal forests, to support the rapid net emission reductions required to avoid exceeding global tipping points of the climate system (Lenton et al., 2008). Indeed, boreal forests have potential for climate change mitigation by holding CO_2 away from the atmosphere stored as carbon for long periods (Pan et al., 2011). To which extent carbon retention potential and wood production clash is a key question when planning management strategies for the future.

To evaluate the potential for climate change mitigation of forest managements we need to quantify the forest's wood production and subsequent fate of harvested wood products and the associated carbon. A commonly employed metric of carbon sequestration is the net ecosystem carbon gain over a certain amount of time (Pukkala, 2020, Sterck et al., 2021). This metric ignores the carbon transit time outside the atmosphere, i.e., the time span between the carbon fixation via photosynthesis and its release back to the atmosphere. Yet, the transit time is the period during which this carbon does not contribute to the radiative effects of greenhouse gases emitted to the atmosphere (i.e., the Global Warming Potential; Shine et al. 1990). Knowing both the amount and time the carbon spends outside the atmosphere is key to quantify the *avoided* radiative effect (Sierra et al., 2021) by storing the carbon in ecosystems or wood products, and hence the climate change

mitigation potential. Also the fate of harvested carbon and of legacy carbon, i.e., carbon already in the ecosystem and wood products at the beginning of the forest management cycle, needs to be considered. Harvested carbon does not immediately return to the atmosphere but spends considerable time as wood products (Schulze et al., 2020), potentially defining whether ultimately a managed forest is a carbon source or sink (Liski et al., 2001). The fate of legacy carbon is of particular relevance to climate change mitigation potential when management is applied to old-growth forests (Luyssaert et al., 2008). Despite their importance for climate change mitigation, these aspects have so far not been jointly and systematically quantified when assessing alternative forest management scenarios.

Forest management strategies differ in their synergies and trade-offs among economic, biodiversity, and climate change mitigation targets (Pohjanmies et al., 2017). Currently, the predominant approach to timber production in boreal forests is even-aged forestry with one to three thinnings to promote tree growth, followed by a clear cut at the end of the rotation and subsequent regeneration (Pohjanmies et al., 2017). Selection harvesting to maintain continuous forest cover of mixed-age, mixed-size and multi-species stands have been suggested as alternatives to better address environmental and societal concerns stemming from even-aged management (Kuuluvainen et al., 2012, Larsen et al., 2022, Kellomäki, 2022). Selection harvesting (also called mixed-aged/uneven-aged management or continuous-cover management) better mimics natural disturbances than clear-cut based harvesting, in regions where stand-replacing natural disturbances are uncommon (e.g., in Fennoscandia) (Gromtsev, 2002, Shorohova et al., 2009, Kuuluvainen et al., 2011). Even where stand-replacing disturbances (e.g., wildfires) occur, clear-cut based harvesting does not ensure a suitable share of late-successional forest (Bergeron et al., 2004).

The consequences of age and species diversity for production are site- and species-specific (Pukkala et al., 2009, Mikola, 1984, Lähde et al., 2010,

Huuskonen et al., 2021, Holmström et al., 2018). Results are also mixed regarding ecological and economical outcomes, and dependent on spatial and temporal timescales considered and the quantification approach (Kuuluvainen et al., 2012). Furthermore, how even-aged and mixed-aged and mixed-species management strategies differ in their climate change mitigation potential remains unclear if considering only the amount of carbon sequestered and not also the transit time. Importantly, we do not know whether and to what extent ensuring both short- and long-term carbon sequestration reduces biomass and/or wood production Pohjanmies et al. (2017).

The decade-long time scales typical for boreal forest rotation make modelling a powerful tool to evaluate the effects of management choices on specific services. Most ecological growth and yield models of boreal forests focus mainly on wood production (SORTIE, Pacala et al. 1996; CROBAS, Mäkelä 1997; 3PG, Landsberg and Waring 1997) and less frequently on carbon sequestration (Pukkala 2014, Pukkala 2020). Furthermore, most existing models are conceptualized for even-aged management (Kuuluvainen et al., 2012) and do not allow to explore mixed-species or mixed-aged stands (e.g. Hynynen et al., 2002). Models of forest growth applicable to both even- and mixed-aged stands generally compute diameter increment or distribution without accounting for carbon fluxes between tree organs (Kolström, 1993, Martin Bollandsås et al., 2008, Pukkala et al., 2009). Importantly, none of these models allows to track carbon and compute the transit time, i.e., the time that the carbon spends away from the atmosphere, including the role of the fate of harvested wood products. For an effective quantification of climate change mitigation potential, we need a model that describes the carbon stocks and fluxes in the forest during the entire rotation and beyond, including the legacy carbon from before the beginning of the rotation and wood product use after harvest. The model also needs to allow the exploration of a variety of management scenarios, including mixed-aged and mixed-species ones.

Here we develop a model that follows the carbon path from the moment of its photosynthetic fixation from the atmosphere, through its fate in the forest, until the moment it returns to the atmosphere by respiration or wood-product burning. With the help of this model, we quantify wood production, carbon sequestration, and the climate change mitigation potential based on carbon transit time. We ask:

- How do management scenarios rank differently when considering transit time-based climate change mitigation potential vs carbon sequestration?
- How important is the fate of harvested wood products when assessing carbon sequestration and climate change mitigation potential?
- Are there trade-offs across management scenarios between the capacity of forests to produce biomass and sequester carbon and keep it away from the atmosphere ?

While our model is general, we here focus on pure and mixed Scots pine (*Pinus sylvestris*) and Norway spruce (*Picea abies*) stands under current climate conditions for southern Finland. As examples, we consider four management scenarios during an 80 yr rotation: a continuous-cover, mixed-age pine forest and even-aged mono- (pine or spruce), or mixed-species (pine and spruce) stands established after clear-cutting.

2. Materials and methods

We develop and parameterize a mass-balanced, process-based compartmental model, where the forest and wood-product carbon cycle is described by a system of nonlinear nonautonomous ordinary differential equations (Section 2.1). To demonstrate the model capabilities, we compare four boreal forest management scenarios (Section 2.3), with reference to their wood production and carbon sequestration as net carbon gain. We also evaluate the climate change mitigation potential based on the carbon transit time, i.e., the time during which the carbon remains in the system and hence away from the atmosphere (Section 2.2).

2.1. Model description

The model describes the carbon dynamics in a horizontally homogeneous forest stand comprising n different *MeanTree*s competing for light. Each *MeanTree* i represents a cohort of trees of density N_i (ha^{-1}), identical in species, age, and size. Different *MeanTree*s can differ in these properties, allowing to describe not only even-aged mono-specific forest stands, but also mixed-aged and/or mixed-species stands. The carbon dynamics and growth of each *MeanTree* are modeled combining a physiologically-based carbon fixation and statistical descriptions of the tree allometry. For the allometry, we developed an extension of the Allometrically Constrained Growth and Carbon Allocation model (ACGCA, Ogle and Pacala, 2009). Compared with the original formulation, our novel allometric description explicitly considers the carbon allocation to tree organs based on statistical allometries derived from large experimental data (Lehtonen, 2005, Repola, 2009, Repola and Ahnlund Ulvcrona, 2014). The model describes carbon stocks and fluxes entering the system via photosynthetic CO_2 fixation and then exchanged among the carbon pools within each *MeanTree*, three soil carbon pools and two wood-product carbon pools, and eventually released back to the atmosphere. The key state variables of the model are the carbon contents of each

pool (Table 1).

The model consists of four inter-linked modules: 1) a photosynthesis module, computing the annual gross primary productivity of each *MeanTree* (GPP_i), based on the Atmosphere-Plant Exchange Simulator (APES, Launiainen et al. 2015); 2) a tree module, allocating GPP_i to the organs of *MeanTree i* as structural and nonstructural biomass, describing tree-internal and -external fluxes such as growth and maintenance respiration and tissue turnover based on the Allometrically Constrained Growth and Allocation Model (ACGCA, Ogle and Pacala 2009) but with carbon allocation driven by statistical allometries derived from forest inventory data; 3) a soil carbon module; and 4) a forest management module, describing the rules for planting and harvesting of *MeanTree*s (Fig. 1) in specific scenarios and the fate of harvested wood as wood products. The photosynthesis module is solved at half-hourly timescale, while the other modules have annual time step. The complete model description and its parameterization is provided in the Supplementary Information (SI, Section A): only the most salient features are discussed here. Environmental conditions (model forcing) and carbon dynamics parameters are provided in SI, Section B.

2.1.1. Photosynthesis module

The photosynthesis module (SI, Section A.1) computes carbon and water fluxes in the forest stand, considering competition for light among the *MeanTree*s. The module provides the *MeanTree* annual GPP_i - the carbon input to the tree module. The stand structure, i.e., the maximum leaf-area index (LAI) and leaf-area density profiles and heights of each *MeanTree*, are provided by the tree module (Section 2.1.2) at the beginning of each year. The light environment and leaf photosynthesis and transpiration rates are solved separately for the sunlit and shaded parts of each canopy layer (1 m height each), using well-established biogeochemical models and stomatal optimality principles (Farquhar et al., 1980, Medlyn et al., 2012, Launiainen et al., 2015). The photosynthesis module includes sub-models to account

Tree carbon pools	
E	transient, available for growth and maintenance
B_L	leaf biomass
C_L	labile, stored as leaf glucose
B_R	fine root biomass
C_R	labile, stored as root glucose
B_{OS}	"other" sapwood
B_{OH}	"other" heartwood
B_{TS}	trunk sapwood
B_{TH}	trunk heartwood
C_S	labile, stored as sapwood glucose
Soil carbon pools	
Litter	fast litter
CWD	coarse woody debris
SOC	soil organic carbon
Wood-product carbon pools	
WP_S	short-lasting wood products
WP_L	long-lasting wood products

Table 1: State variables of the different model components ($\mathrm{gC\,m^{-2}}$).

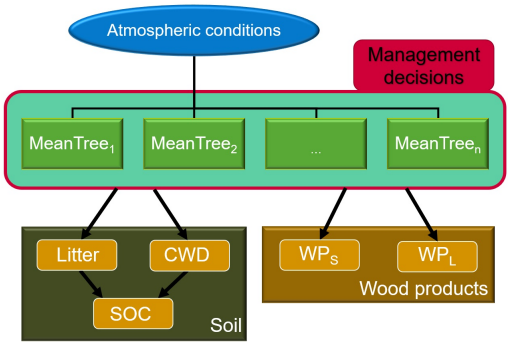

Figure 1: Scheme of the model. Several *MeanTrees* (green boxes) interact with the soil components (dark green box) and the wood product components (brown box). The atmospheric conditions are the forcing of the carbon dynamics. The photosynthesis module quantifies for each *MeanTree* i the annual GPP_i to be distributed to ten tree carbon compartments (carbon pools shown in Fig. 2). Management decisions (i.e., planting, thinning, and cutting) are applied to each *MeanTree* and affect the stand composition and tree carbon distribution to soil and wood-product pools.

for the seasonal leaf-area dynamics and photosynthetic acclimation (Launiainen et al., 2015, 2019), and the feedback of restricted soil water availability in the root zone to leaf gas-exchange (Launiainen et al., 2022). The root zone is described as a single water storage and is equally accessible to each *MeanTree*.

2.1.2. Tree module

The tree module (SI, Section A.2) describes the partitioning of the annual GPP to maintenance and growth of a *MeanTree*'s organs (Fig. 2). All tree module variables are shown in SI, Table A.2.

Each *MeanTree* has ten carbon pools, representing structural (B) and nonstructural (C) carbon in leaves (B_L, C_L), fine roots (B_R, C_R), coarse roots and branches (subscript O, i.e., "other") sapwood (B_{OS}), and heartwood (B_{OH}), as well as the trunk (subscript T) sapwood (B_{TS}) and heartwood (B_{TH}). Coarse roots and branches and the trunk share a single nonstructural labile storage pool C_S, and carbon input from photosynthesis is temporarily stored in a transient pool E.

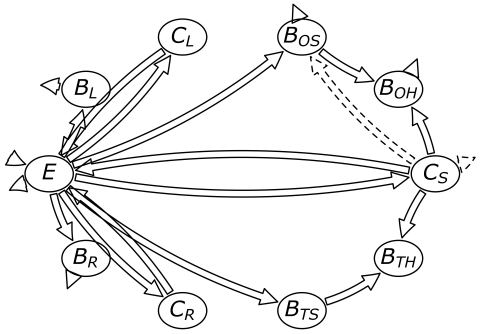

Figure 2: Complete carbon model of a *MeanTree*. Symbols inside the pools are the state variables of the model's tree module (Table 1). In the "static" and "shrinking" states, there is an additional flux from the labile carbon storage (C_S) to B_{OS} to support the regrowth of "other" wood. The the associated growth respiration flux leaves from C_S (dashed arrows).

At the beginning of the new year, the GPP from the previous year is placed in the transient pool E. Losses from this pool occur via maintenance respiration (R_M) of leaves, fine roots, sapwood, and growth respiration. Respired tree carbon returns directly to the atmosphere. Tissues are also lost at tissue-specific rates due to senescence. When senescing biomass leaves the *MeanTree*, the associated carbon in the labile storage pool returns to the transient pool E, where it becomes available again for allocation during the subsequent year.

Thinning and cutting events reduce the number of trees (N_i) represented by a *MeanTreei*. Part of the carbon stored in the harvested biomass is turned into short- (WP_S) or long-lasting (WP_L) wood products (SI, Section A.5), while the cutting residues are either left on site (litter input for soil module) or can become short-lasting bioenergy (part of WP_S) .

The amount of carbon available for allocation after the annual maintenance respiration is $C_{\mathrm{alloc}}\,\Delta t := E - R_M\,\Delta t$, where $\Delta t = 1\,\mathrm{yr}$. When the tree is healthy, its allocation to labile storage, tissue growth, and growth respira-

tion is based on species-specific statistical models describing the dependence of the *MeanTree* organs' biomasses on its diameter at breast height (dbh) (SI, Section A.3.1. These data-driven dynamic relationships overcome a limitation of the original ACGCA model, where the tree allometries were defined by time-invariant parameter values (SI, Section A.3.2). For simplicity, the species-specific fine root-to-leaf biomass ratio ρ_{RL} is assumed constant.

With the allometrically-based information on tree organ biomasses based on dbh, we apply an iterative root-search algorithm to identify the annual radial growth Δdbh such that all available carbon ($C_{\mathrm{alloc}}\,\Delta t$) is used to regrow tissue lost by senescence and to grow new tissue. The density ρ_W of newly produced sapwood and the sapwood to heartwood ratio are determined dynamically so that the trunk biomass follows the external allometric relationships.

The carbon allocated to leaves is split in three components, tissue growth (B_L), transfer into the labile storage pool (C_L), and growth respiration (G_L), so that the ratio of labile storage to leaf structural biomass remains constant (δ_L). The same approach is applied to fine roots (B_R, C_R, δ_R). Conversely, for "other" and trunk, who share a common labile storage pool (C_S), the ratio of labile storage to structural biomass is variable and depends on the density of newly produced sapwood (ρ_W) and species-dependent sapwood parameters (SI, Tables A.3 and A.4). Additional carbon fluxes within the *MeanTree* are related to labile storage returning to the transient pool when associated structural biomass is lost due to senescence.

Should the available photosynthetic carbon input be low, the tree reverts to a "static" physiological state (see SI, Section A.4), in which the regrowth of senescent leaves and fine roots is prioritized, and with $\Delta\mathrm{dbh} = 0$ the regrowth of lost sapwood and heartwood of coarse roots and branches exploits carbon resources from the labile storage pool C_S. If $C_{\mathrm{alloc}}\,\Delta t$ is insufficient to cover the costs of replacement of senescing leaves and fine roots, the tree switches to a "shrinking" state, where the tree loses leaf and fine root biomass

proportionally to the needs, while "other" organs are regrown from the labile storage. If in subsequent years $C_{\text{alloc}}\,\Delta t$ is again sufficient to cover all the carbon needs (e.g., due to stand management or favorable environmental conditions), the tree reverts directly to the "healthy" state. If instead the GPP remains low, and the labile carbon storage C_S depletes, the *MeanTree* dies.

2.1.3. Soil module

The soil module (Fig. 1; SI, Section A.7) describes soil carbon dynamics based on three pools: fast decomposing litter (Litter), slowly decomposing coarse woody debris (CWD), and soil organic carbon (SOC). We included a single soil organic carbon pool because we focus on carbon in the topsoil. Our interest in yearly to decadal timescales limits the need for a separation into fast and slow decomposing soil organic carbon pools (Manzoni and Porporato, 2009). The carbon input from the *MeanTree*s' senescing leaves and fine roots enters the soil module as litter fall through the Litter pool, while sapwood and heartwood carbon due to senescence enter the coarse woody debris pool (CWD). Further soil carbon input occurs from cutting residues that are not removed from the ecosystem (see SI, Section A.5).

For simplicity, the decay rates and transfer coefficients between pools are set constant, i.e., we currently neglect the role of inter-annual climatic variability. Decomposing carbon from Litter and CWD is partly directly respired to the atmosphere and partly moved to SOC, from where it is eventually respired.

2.1.4. Management and wood product module

The forest management module defines the management actions applied to *MeanTree*s in the stand. Management includes i) initial planting of new *MeanTree*s of given species and initial size (dbh_i) at a density N_i; ii) thinning (i.e., partial reduction of a *MeanTree*'s N_i); iii) cutting (complete removal of the *MeanTree*), and iv) potential replanting of a new *MeanTree* after

cutting. The cutting can be planned or caused by the death of the *MeanTree*, which happens when in the "shrinking" state the labile storage pool (C_S) is depleted.

When a tree in a stand is removed by thinning or cutting, the tree carbon is transferred to the soil and to short- and long-term wood-product pools depending on the tree's species, size and its taper curve (see SI, Section A.5). The carbon transferred to wood-product pools is removed from the stand.

2.1.5. Mathematical formulation of the model

The model can mathematically be represented as a compartmental system (Anderson, 1983, Jacquez and Simon, 1993, Luo and Weng, 2011, Sierra and Müller, 2015, Sierra et al., 2018) and described by a d-dimensional system of nonlinear and nonautonomous ordinary differential equations,

$$\begin{aligned} \frac{\mathrm{d}}{\mathrm{d}\,t}\,\mathbf{x}(t) &= \mathrm{B}(\mathbf{x}(t),t)\,\mathbf{x}(t) + \mathbf{u}(\mathbf{x}(t),t), \quad t > 0, \\ \mathbf{x}(0) &= \mathbf{x}^0. \end{aligned} \tag{1}$$

Here $\mathbf{x}(t) \in \mathbb{R}^d$ ($\mathrm{gC\,m^{-2}}$) is the vector of carbon pools at time $t \geq 0$ (yr), $\mathbf{x}^0$ gives their initial sizes at time $t = 0$ and the vector-valued function $\mathbf{u}$ ($\mathrm{gC\,m^{-2}\,yr^{-1}}$) represents the gross photosynthetic input to the system ($\mathrm{GPP} = \sum_{i=1}^{n} \mathrm{GPP}_i$). The matrix-valued function B (compartmental matrix) governs the internal carbon cycling and the release of carbon from the system to the atmosphere. The matrix entry B_{ij} denotes the rate of carbon transferred from pool j to pool i. The dimension of the equation system is $d = 10\,n + 3 + 2$, comprising ten pools for each of the n *MeanTree*s, three soil carbon pools, and two wood-product pools.

Fluxes ($\mathrm{gC\,m^{-2}\,yr^{-1}}$) from pool j to pool i at time t are given by

$$F_{ij}(t) = B_{ij}(\mathbf{x}(t),t)\,x_j(t), \quad t \geq 0. \tag{2}$$

By running the (discretely implemented) model and storing all pool sizes and

fluxes through time, we can reconstruct the compartmental matrices $\mathrm{B}(t_k)$ (Metzler et al., 2020) for all time steps t_k. This allows us to compute the transit times of carbon through the system (Rasmussen et al., 2016, Metzler et al., 2018) and to quantify the climate change mitigation potential of the system (Bolin and Rodhe, 1973, Sierra et al., 2017, 2021) (see Section 2.2.2).

The solution of Eq. (1) is given by (Brockett, 2015, Theorem 1.6.1)

$$\mathbf{x}(t) = \Phi(t,0)\,\mathbf{x}^0 + \int_0^t \Phi(t,\tau)\,\mathbf{u}(\tau)\,\mathrm{d}\tau, \tag{3}$$

where the first term on the right hand side is the remaining legacy carbon at time t and the second term is the amount of carbon that has entered the system and remained since the beginning of the simulation. Legacy carbon, given by $\mathbf{x}^0$, is the initial amount in the vegetation biomass, the soil, and the wood products at time $t = 0$. The matrix-valued function Φ denotes the state-transition operator given as the numerical solution of the matrix equation

$$\begin{aligned} \frac{\mathrm{d}}{\mathrm{d}\,t}\Phi(t,s) &= \mathrm{B}(t)\,\Phi(t,s), \quad 0 < s \leq t, \\ \Phi(s,s) &= \mathrm{I}, \end{aligned} \tag{4}$$

where I is the identity matrix. For a vector $\mathbf{x}(s)$ of carbon stocks in different pools at time s, the vector $\Phi(t,s)\,\mathbf{x}(s)$ describes the remaining mass (not yet returned to the atmosphere) and its distribution over the pools at time $t \geq s$.

2.2. Performance metrics for management scenarios

We assess the performance of alternative scenarios by measuring their wood production, carbon sequestration and climate change mitigation potential.

2.2.1. Wood production

The short-lasting (Y_S) and long-lasting (Y_L) wood-product yields until time T are quantified as the integrated carbon fluxes entering the short-

and long-lasting wood-product pools (WP_S and WP_L), respectively. Let S and L be the indices of WP_S and WP_L in the carbon content vector $\mathbf{x}$, i.e., $x_S = \mathrm{WP}_S$ and $x_L = \mathrm{WP}_L$. Then

$$\begin{aligned} Y_S(T) &= \int_0^T \sum_{j \neq S} B_{Sj}(t)\, x_j(t)\, \mathrm{d}t \quad \text{and} \\ Y_L(T) &= \int_0^T \sum_{j \neq L} B_{Lj}(t)\, x_j(t)\, \mathrm{d}t. \end{aligned} \tag{5}$$

2.2.2. Carbon sequestration and climate change mitigation potential

We quantify carbon sequestration and the potential for climate change mitigation via three metrics, measuring the net carbon gain and the time that carbon is held in the system (i.e., away from the atmosphere). We contrast the results relative to the entire system (including wood products) with those for the forest stand only, because the wood products can be a crucial factor for whether a forest stand subject to a specific management scenario is a carbon sink or source (Liski et al., 2001).

We measure carbon sequestration via the Integrated Net Carbon Balance (INCB). At time T, $\mathrm{INCB}(T)$ quantifies the net gain or loss over a certain time interval $[0, T]$, but without considering *when* the carbon uptake or release have taken place. It is quantified as the integrated carbon inputs to the system minus the integrated outputs from the system over a certain period of time. The INCB can also be described as the total carbon stocks at time T minus the total stocks at time $t = 0$. Hence,

$$\mathrm{INCB}(T) = \int_0^T \|\mathbf{u}(t) - \mathbf{r}(t)\|\, \mathrm{d}t = \|\mathbf{x}(T)\| - \|\mathbf{x}^0\|, \tag{6}$$

where the carbon inputs at a generic time t are given by $\|\mathbf{u}(t)\|$, with $\|\mathbf{u}(\mathbf{t})\| =$

$\sum_i |u_i(t)|$, and the carbon outputs from pool j are given by

$$r_j(t) = -\sum_i B_{ij}(t)\, x_j(t). \tag{7}$$

A second metric is the Integrated Inputs Transit Time (IITT, called CS in Sierra et al. 2021). It accounts both for the amount of photosynthetically fixed carbon during the rotation and for the time that this carbon spends outside the atmosphere (i.e., not acting as greenhouse gas), but ignores the storage and release of legacy carbon. The IITT up to time T is given by

$$\mathrm{IITT}(T) = \int_0^T \int_0^t \|\Phi(t,\tau)\, \mathbf{u}(\tau)\|\, \mathrm{d}\tau\, \mathrm{d}t. \tag{8}$$

To overcome the limitation of IITT not considering legacy carbon, we consider a third metric, the Integrated Carbon Stocks (ICS), based on the same concept as IITT, but including also the fate of legacy carbon, which is treated as entering the system at $t = 0$. The ICS is computed as

$$\mathrm{ICS}(T) = \int_0^T \|\Phi(t,0)\, \mathbf{x}^0\|\, \mathrm{d}t + \mathrm{IITT}(T) = \int_0^T \|\mathbf{x}(t)\|\, \mathrm{d}t. \tag{9}$$

While the dimension of INCB is mass, the dimension of both IITT and ICS is mass $\times$ time, because we integrate a mass over time. All three quantities increase as more carbon enters the system, but only the latter two increase if this carbon spends more time in the system. Consequently, IITT and ICS can be used to effectively assess climate change mitigation potential, while INCB is suitable only to quantify carbon sequestration.

2.3. Simulations and management scenarios

Starting with empty carbon pools, a common 160 yr spinup (SI, Section C) consisting of a mono-specific mixed-aged pine forest of four *MeanTree*s

is run to initialize the stand structure and tree, soil and wood-product carbon pools (C). From this single initial state, we consider alternative management scenarios leading to different stand compositions:

- **Mixed-aged pine stand**
  We maintain a mixed-aged pine stand with a continuous canopy cover. At the beginning of the rotation, the oldest *MeanTree* from the spinup is cut and replanted. Thereafter, every 20 yr the oldest *MeanTree* is cut and replanted, thus maintaining four *MeanTree*s of ages ranging from 0 to 80 yr and differing among them by 20 yr.

- **Even-aged single-species stand (pine or spruce)**
  After a clear-cut of the spinup stand, four *MeanTree* pines (or spruces) are replanted. We use four slightly differently sized *MeanTree*s at planting (dbh = 1.0, 1.2, 1.4, 1.6 cm) to approximate the initial size distribution. The effects of small initial size differences can compound in time due to unequal access to light.

- **Even-aged mixed-species (pine and spruce) stand**
  After a clear-cut of the spinup stand, we plant two pine *MeanTree*s and two spruce *MeanTree*s. For both species the initial dbh values are 1.2 and 1.4 cm.

In all even-aged scenarios, the *MeanTree* i initially comprises $N_i = 500\,\mathrm{ha}^{-1}$ identical trees, while in the mixed-aged scenario $N_i = 375\,\mathrm{ha}^{-1}$. All scenarios start with the same initial condition, last for 80 yr, and end with a final felling of all trees, where all tree carbon is transferred to soil- or wood-product pools. The same environmental forcing is used in all simulations, consisting of recycled 20 yr meteorological data from Hyytiälä SMEAR II-research station (61.51°N, 24.00°E) in Southern Finland (Launiainen et al., 2022).

In even-aged scenarios a pre-commercial thinning is executed as soon as the mean tree height reaches 3.0 m. All *MeanTree*s are then equally thinned such that the total stand density is reduced from 2000 to 1500 trees per

hectare, which equals the stand density of the mixed-aged scenario. When the stand basal area (SBA) reaches $25\,\mathrm{m}^2\,\mathrm{ha}^{-1}$ during any simulation, all *MeanTree*s are uniformly thinned to reduce SBA to $18\,\mathrm{m}^2\,\mathrm{ha}^{-1}$, resembling current recommendations in Finland (Kellomäki, 2022, Kellomäki et al., 2008, Yrjölä, 2002). Such thinning is skipped if a scheduled cutting (in the mixed-aged pine scenario) or the final felling (in all simulations) is planned for within the following 10 yr.

In the mixed-aged pine scenario, when a *MeanTree* i is cut, it is replanted at density $N_i = 375$ trees per hectare with a delay of 4 yr. This delay in replanting is implemented because the allometric relationships used here are not valid below dbh = 1.0 cm. Hence, the four years of delay approximate the time that seedlings need to grow to a size of dbh = 1.0 cm.

When the forest stand becomes increasingly dense, a *MeanTree* might not gather enough carbon from photosynthesis to sustain maintenance and regrowth of senescent biomass. In this case the growth of the *MeanTree* is reduced, and it uses its labile storage (C_S) to regrow senescent coarse roots and branches (see SI, Section A.4). Upon depletion of C_S, the *MeanTree* dies and is removed from the stand by cutting it down and transferring its carbon to the soil and to wood products. This process resembles self-thinning, and is called *emergency removal* of the *MeanTree*. At the time of an emergency removal of a dying *MeanTree*, the remaining stand is also equally thinned down to SBA = $18\,\mathrm{m}^2\,\mathrm{ha}^{-1}$ in order to minimize the number of thinnings and cuttings that have to be executed.

3. Results

3.1. Dynamics of stand attributes and biomass under different management scenarios

Despite the common starting point at the end of the spinup, the stand attributes and carbon pool dynamics differ significantly among the management scenarios (Fig. 3).

All the even-aged scenarios involve an initial clear cut of the spinup trees and replanting. As a result, mean stand dbh, stand basal area and tree carbon stocks are low compared with the mixed-aged pine forest at the beginning of the simulation (Fig. 3). The replanted trees then grow until SBA reaches the $25\,\mathrm{m}^2\,\mathrm{ha}^{-1}$ thinning threshold or a *MeanTree* dies due to persistent light limitations and is subsequently cut. Which event occurs first and its timing depends on the scenario. In the even-aged pine scenario (orange lines) the SBA reaches the thinning threshold after 50 and 60 yr; the uniform thinning of all four *MeanTree*s reduces stand density to 1056 and further to 740 trees ha^{-1}, respectively. In the even-aged spruce scenario, emergency removals due to persistent light-limitations occur after 40 and 49 yr in the suppressed (small) spruces. The remaining *MeanTree*s are equally thinned to SBA $= 18\,\mathrm{m}^2\,\mathrm{ha}^{-1}$. After 61 yr the SBA thinning threshold is reached and the two remaining *MeanTree*s are equally thinned. After 65 yr another emergency removal occurs, leaving only one *MeanTree* till the end of the rotation, without any additional thinning. The final stand density in even-aged spruce scenario is 202 trees ha^{-1}. In the mixed-species scenario (red lines) SBA reaches the $25\,\mathrm{m}^2\,\mathrm{ha}^{-1}$ thinning threshold after 42, 52, and 61 yr; the uniform thinning of all *MeanTree*s subsequently reduces stand density to 1069, 765 and finally to 547 trees ha^{-1}. In all scenarios, when thinning occurs, tree density declines and SBA (Fig. 3B) temporarily decreases. In case of an emergency removal, mean dbh increases (Fig. 3A) because the smallest *MeanTree* is removed.

The mixed-aged pine forest scenario has radically different stand dynamics (blue lines in Fig. 3), because only the tallest *MeanTree* is cut down at the beginning of the simulation and one new small *MeanTree* seedling is replanted. The mean dbh (Fig. 3A) decreases at removal of the largest tree and more so when the seedlings are replanted 4 years later, although changes are small compared with even-aged forests. Also the stand basal area (Fig. 3B) and the total tree carbon stock (Fig. 3D) drop upon removal of the dom-

inant *MeanTree*. The initial cutting of the oldest tree causes a transfer of $2.3\,\mathrm{kgC\,m^{-2}}$ from the tree pools to the soil pools (Litter and CWD), whereas $3.2\,\mathrm{kgC\,m^{-2}}$ are transferred from tree pools to wood-product pools (WP_S and WP_L). Every 20 yr the oldest *MeanTree* has a dbh around 20 cm and is cut and substituted by seedlings, leading to periodicity in SBA.

3.2. Wood production

The mixed-aged pine scenario is the most productive over the 80-yr rotation, having the largest cumulative yield of short- and long-term wood products ($Y_S + Y_L = 13.6\,\mathrm{kgC\,m^{-2}}$). Between 1.7 and $2.0\,\mathrm{kgC\,m^{-2}}$ are transferred to the soil pools, and between 2.3 and $2.7\,\mathrm{kgC\,m^{-2}}$ to the wood-product pools at each cutting. At the end of the rotation, all trees are cut down and 2.7 and $3.0\,\mathrm{kgC\,m^{-2}}$ are transferred to the soil and wood products, respectively. This scenario is used as reference in further comparisons (see values in Fig. 4A and Table 2). In terms of total wood products, the even-aged pine scenario ranks second and is about 88 % as productive in total and 94 % and 83 % in terms of short- and long-lasting wood products, respectively. The even-aged spruce scenario is the least productive, with total wood products of 69 % and short- and long-lasting products of 45 % and 83 % of that of the mixed-aged pine.

While in both the mixed-aged and the even-aged pine stands ca. 60 % of the harvested wood met the dbh and length criteria implemented for long-lasting wood products, additional mixed-aged pine simulations showed that this percentage strongly increases when stand density decreases, from $N = 2000$ to $N = 1000\,\mathrm{ha^{-1}}$. This, however, reduces the total carbon stock in the system, climate change mitigation potential and the yield of short-lasting wood products (SI, Fig. E.2).

3.3. Carbon sequestration and climate change mitigation potential

The modelled dynamics of dbh, SBA, carbon stocks, and wood production (Fig. 3) offer insights into the carbon sequestration and the potential for

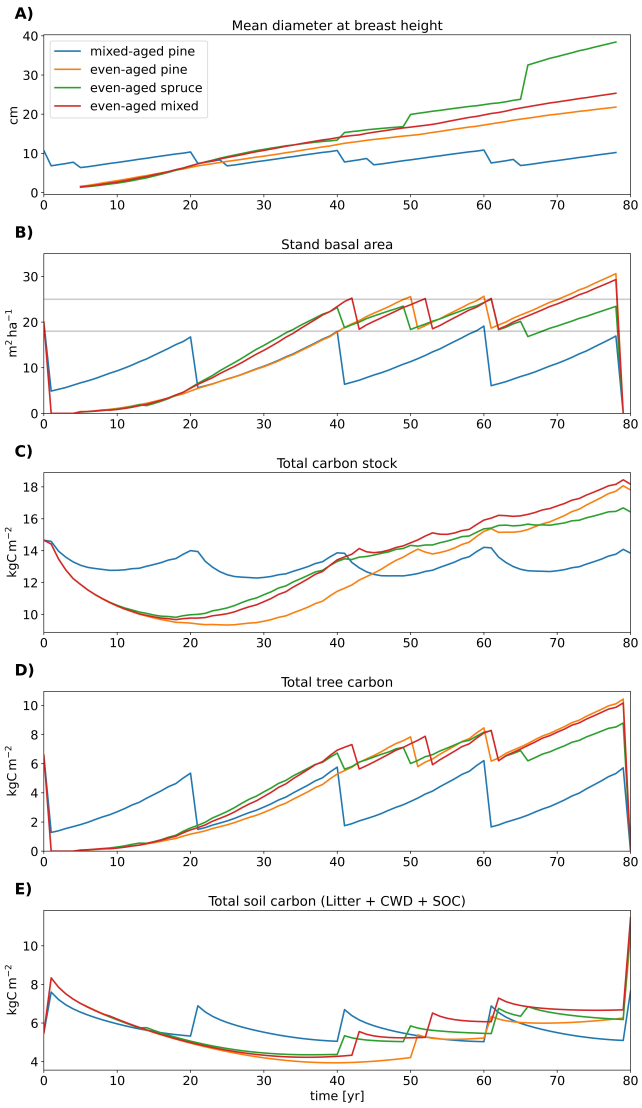

Figure 3: Temporal evolution of key model outputs (panels) for the four management scenarios (colors): A) Tree mean diameter at breast height (cm), averaged over all trees in the stand. B) Stand basal area ($m^2\,ha^{-1}$). Grey lines correspond to SBA = 25 and SBA = $18\,m^2\,ha^{-1}$, i.e., the upper and lower ends of SBA-dependent thinning. C) Total carbon stock including trees, soil, and wood products ($kgC\,m^{-2}$). D) Total tree carbon stock ($kgC\,m^{-2}$). E) Total soil carbon (Litter + CWD + SOC) ($kgC\,m^{-2}$). A detailed attribution of tree carbon to single *MeanTree*s is shown in SI, Fig. E.1

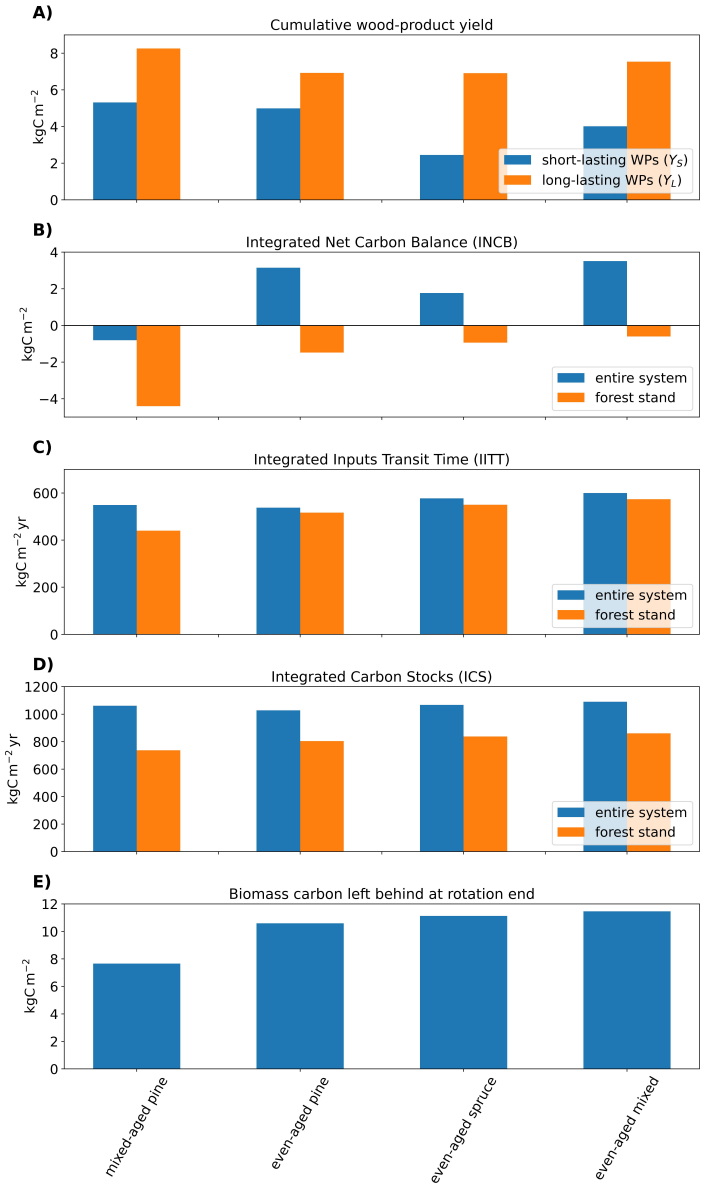

Figure 4: Performance of management scenarios over the whole rotation when wood-product carbon is included (blue bars), and when excluded (forest stand; i.e., tree and soil carbon only; orange bars). Panels refer to the following metrics: A) Integrated wood-product yield as short-lasting (Y_S) and long-lasting (Y_L) wood-products (Eq. 5). B) Integrated Net Carbon Balance (INCB, Eq. 6). C) Integrated Inputs Transit Time (IITT, Eq. 8). D) Integrated Carbon Stocks (ICS, Eq. 9). E) The carbon left at the site after the clear cut at the end of the rotation; includes carbon in litter, coarse woody debris, and soil organic carbon.

climate change mitigation.

The initial clear cut in the even-aged scenarios reduces tree carbon stocks and ecosystem carbon uptake, while wood-product and soil carbon is lost as CO_2 (Fig. 3D). During the first 18 (spruce and mixed) to 25 yr (pine) the total carbon stock (trees + soil + wood products) in the system decreases by $\approx 5\,\mathrm{gC\,m^{-2}}$, and at the minimum it is less than two thirds of the pre-harvest level. The soil carbon stock is lowest ca. 40 yr after the clear cut, approximately half of the initial value. Later in the rotation even-aged pine and mixed-species scenarios lead to higher total carbon stock than the continuous-cover scenario (Fig. 3C). About 50 yr in the rotation the initial losses are regained (Fig. 3E).

While the differences in total tree carbon stocks between the three even-aged scenarios are small at the end of the rotation (Fig. 3D), the total carbon stock is highest in the even-aged mixed scenario, followed by even-aged pine and even-aged spruce (Fig. 3C). Conversely, the total carbon stock recovery early in the rotation is most rapid in the fast-growing young spruce stand. In the even-aged management scenarios, it takes $42 - 46$ yr before the total carbon stocks (Integrated Net Carbon Balance, INCB, Fig. 3B) have recovered from the initial clear-cut loss and are at the level of the mixed-aged (continuous cover) scenario. However, it takes 68 yr in mixed-species forest and 70 yr for spruce to compensate the lost climate change mitigation potential, if considering the time during which carbon is retained from the atmosphere (Integrated Inputs Transit Time, IITT, Fig. 5C). The even-aged pine forest does not compensate for that within the simulated 80 yr rotation.

An even more pronounced difference among management scenarios emerges when considering also the fate of legacy carbon (Integrated Carbon Stocks, ICS, Fig. 5D), i.e., the carbon that was in trees, soil, or wood products at the beginning of the simulation. Even-aged mixed and spruce scenarios are level with the mixed-aged simulation only after 72 and 78 yr, respectively. Both IITT and ICS in the even-aged pine scenario fail to recover over the entire

rotation.

When accounting for carbon retention times of wood products (Table 2, Entire system) instead of considering retention times only in trees and soil (Table 2, Stand only), the absolute values of both IITT and ICS increase. Relative increases by including wood products are clearly highest in the mixed-aged pine scenario (IITT: +25 %, ICS: +44 %). Also some rankings of the management scenarios change when including wood products (Table 2).

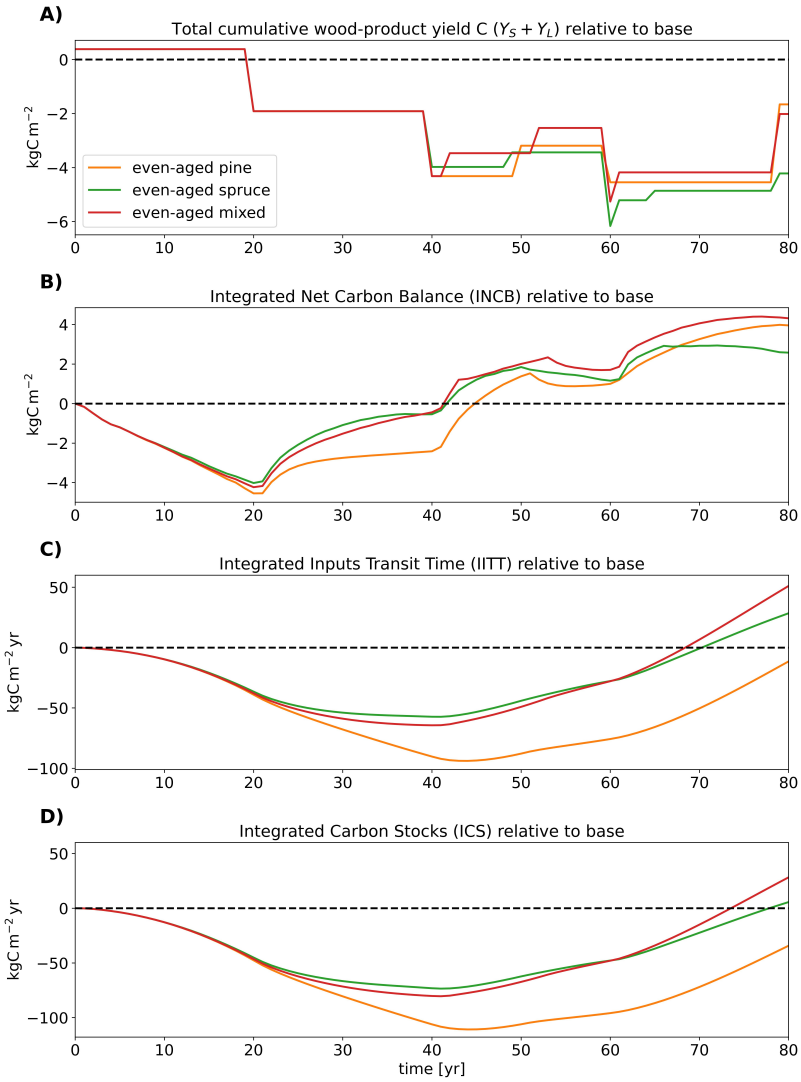

Figure 5: Temporal evolution of wood production, carbon sequestration and climate change mitigation potential metrics. A) Total cumulative wood-product yield carbon ($Y_S + Y_L$, Eq. (5)). B) Integrated Net Carbon Balance (INCB, Eq. (6)). C) Integrated Inputs Transit Time (IITT, Eq. (8)). D) Integrated Carbon Stocks (ICS, Eq. (9)). Values are differences of the even-aged strategies from the mixed-aged scenario.

		Entire system		Stand only	
Metric	**Scenario**	**Rank**	**Value**	**Rank**	**Value**
INCB	mixed-aged pine	4	-0.8	4	-4.4
($\mathrm{kgC\,m^{-2}}$)	even-aged pine	2	3.2	3	-1.5
	even-aged spruce	3	1.8	2	-0.9
	even-aged mixed	1	3.5	1	-0.6
IITT	mixed-aged pine	3	549.0	4	440.0
($\mathrm{kgC\,m^{-2}\,yr}$)	even-aged pine	4	537.5	3	516.4
	even-aged spruce	2	577.4	2	550.1
	even-aged mixed	1	600.0	1	573.4
ICS	mixed-aged pine	3	1061.7	4	737.2
($\mathrm{kgC\,m^{-2}\,yr}$)	even-aged pine	4	1027.5	3	803.8
	even-aged spruce	2	1067.3	2	837.5
	even-aged mixed	1	1090.0	1	860.8
Y_S	mixed-aged pine	1	5.3		
($\mathrm{kgC\,m^{-2}}$)	even-aged pine	2	5.0		
	even-aged spruce	4	2.4		
	even-aged mixed	3	4.0		
Y_L	mixed-aged pine	1	8.3		
($\mathrm{kgC\,m^{-2}}$)	even-aged pine	3	6.9		
	even-aged spruce	4	6.9		
	even-aged mixed	2	7.5		
$Y_S + Y_L$	mixed-aged pine	1	13.6		
($\mathrm{kgC\,m^{-2}}$)	even-aged pine	2	11.9		
	even-aged spruce	4	9.4		
	even-aged mixed	3	11.6		

Table 2: Ranking of management scenarios according to carbon sequestration (INCB) and climate change mitigation potential metrics (IITT, ICS), with respect to the entire system (trees, soil, and wood products) and the stand only (trees and soil), and short-lasting (Y_S), long-lasting (Y_L) and combined ($Y_S + Y_L$) wood-product yield. The values correspond to those in Fig. 4

.

4. Discussion

4.1. Methodological considerations

Boreal forest management strategies have commonly been assessed through their economic perspectives over fixed planning horizons (e.g., $60-100$ yr rotation cycles). The increasing interest in climate change mitigation by forests (Astrup et al., 2018, Triviño et al., 2023) makes such metrics insufficient. To properly assess the climate change mitigation potential of an ecosystem, we must consider the timing of carbon fixation, its release and storage dynamics (i.e., the time that carbon spends outside the atmosphere) over the entire rotation and beyond. Contrasting management scenarios thus requires models that can track the carbon flow from its photosynthetical fixation, through its use in tree metabolism and growth, to its subsequent transfer to other ecosystem components (e.g., the soil) or to wood products.

To address this need, we combined an improved version of the Allometrically Constrained Growth and Carbon Allocation model (ACGCA, Ogle and Pacala, 2009) with photosynthesis and soil modules, and incorporated harvested wood-product pools. Compared with existing tree growth models (see reviews by Hawkes 2000, Le Roux et al. 2001, Busing and Mailly 2004) and allocation schemes (see reviews by Ågren and Wikström 1993, Cannell and Dewar 1994, Lacointe 2000), our model has the advantage of resting on a mass-balanced approach described by discretely implemented ordinary differential equations. Our formulation allows computing the carbon age distributions and transit times directly, quantifying not only how much carbon the forest stand stores but also the *avoided* atmospheric radiative warming effect provided by the prolonged storage of carbon in the ecosystem (Sierra et al., 2021) or in wood products. The quantification of not only the amount of carbon in the system but also the time it spends there is necessary to evaluate the reduction of Global Warming Potential (Shine et al., 1990) for different management scenarios. We employed a detailed process-based photosynthesis model that quantifies carbon fixation at a half-hourly time step

for each *MeanTree* (part of APES, Launiainen et al., 2015). In contrast to forest growth models relying on empirical relationships, our approach allows to describe directly the effects of species traits, soil and climatic conditions, ensuring transferability to other species and regions. The explicit description of the light environment in the canopy enables the consideration of the among-tree competition for light, necessary to simulate mixed-species and mixed-aged forests. As such, we can evaluate also the prospects of currently uncommon management strategies with no historical data to rely on.

Process-based descriptions and mass conservation are applied to compute GPP, respiration, and fluxes between system compartments. Carbon allocation to tree organs is described via empirical allometric equations, linking tree organ biomass to dbh, derived from species-specific forest inventory data (SI, Section A.3.1). Allometric equations are a compromise between a minimalist description and detailed physiology-based functions (Bugmann, 2001). At the same time, employing allometries derived from forest inventory reduces the effects of internal parameter uncertainties, because they ensure that tree carbon allocation is ultimately realistic. The disadvantage is that some parameters lack clear ecophysiological meaning and are hard to estimate independently. The species-specific but fixed parameterization of biomass maintenance and growth costs and the fine root-to-leaf biomass ratio neglect the dynamic behavior of trees in the stand. For instance, a reduction in the fine root-to-leaf biomass ratio (ρ_{RL}) leads to reduced carbon allocation to roots and hence more carbon available for stem growth.

The detailed description of carbon flows within the *MeanTree* also results in allocating carbon from GPP (instead of net primary productivity) to the tree organs and to maintenance respiration (Sierra et al., 2022). This is not only more physiologically correct, but provides a true carbon age distribution for autotrophic respiration, which is comparable with radiocarbon measurements (Carbone et al., 2007, 2013, Muhr et al., 2013). These increasingly available data could support validation or identification of model parame-

ters that are otherwise hard to estimate (e.g., those related to nonstructural carbohydrate pools - δ_L, δ_R, δ_S).

The inclusion of the nonstructural carbohydrate pool C_S enables the assessment of the tree's health status and its response to external stress (Bugmann, 2001), although we employ a simplified description of the transition back to a healthy state. This allows us to consider the effects of light limitations and reduced carbon fixation on tree mortality, and of carbon release upon competition removal via tree death or different thinning practices (see SI, Section A.4). The removal of *MeanTree*s after they have depleted their labile carbon storage under prolonged light limitation mimics self-thinning or thinning from below. Indeed, the modelled stand density in the even-aged spruce and pine scenarios largely follows Reineke's rule (Reineke, 1933) which links density and mean dbh (SI, Fig. E.3), thus lending support to our results.

Our model also allows the analysis of single/mixed-species and even/mixed-aged stands. Species and age mixtures are, however, considered in a simplified way neglecting among-tree competition for water and nutrients and the facilitating effects beyond reduction of competition for light, for instance due to canopy niche complementarity. Furthermore, we assumed that tree allometric relationships are independent of the specific mixture, although in reality mixed-species allometries can deviate from those of single-species stands (Riofrío et al., 2019).

While light, water and temperature limitations are considered, other abiotic and biotic disturbances (e.g., nutrient limitation, pest infestation, wind throw, snow and ice damage) are currently omitted. As such, the estimated carbon sequestration and wood production could be considered a best-case scenario. The modular structure of the model, however, enables additional processes to be easily included or substituted by more detailed descriptions, should data be available. For example, the soil carbon module could be developed to include dynamic decay rates and transfer coefficients between

pools to capture the role of inter-annual climatic variability as in models with more sophisticated structures, such as Roth-C (Jenkinson and Rayner, 1977) or Century (Parton et al., 1987). Similarly, the allometric relationships could be altered to accommodate forests growing in different and changing conditions, via dynamic rules or competition on water and nutrients among the *MeanTree*s.

Sensitivity analysis revealed that growth, stand biomass development, and subsequent tree and soil carbon pool dynamics are most sensitive to parameters relative to sapwood width (SW), wood density (ρ_W), leaf senescence rate (S_L), and maintenance and growth (e.g., R_{mL}, C_{gL}, R_{mS}, C_{gW}; not shown). This underlines the need for accurate data from field experiments. Another integral part of our model is the description of the tree allometry. Currently, the allometric functions are independent of dynamically changing site properties, such as tree density. The model's generality and applicability could be improved by calibrating the model against growth and yield data from national forest inventory (NFI) plots and introducing tree-density dependent rules, e.g., for the dbh-tree height relationship.

Finally, we note that in this work our primary goal was to illustrate the model capabilities in determining climate change mitigation potential and how that contrasts with other, commonly employed performance metrics. Thus, we considered a single initial state and idealized management scenarios. Nevertheless, whether mixed-aged or even-aged management is more productive might depend on the age structure of the initial stand (Gobakken et al., 2008).

4.2. Model evaluation and benchmarking

Most of the model's sub-modules rely on well-established approaches, which have been extensively tested earlier. For example, the photosynthesis module has already been validated for boreal forests in Fennoscandia (Launiainen et al., 2015, Leppä et al., 2020, Launiainen et al., 2019, 2022). The carbon dynamics of the tree module are based on ACGCA, which has been

successfully used in simulations of tree growth (Fell et al., 2018), gap dynamics (Ogle and Pacala, 2009, Fell and Ogle, 2018), and labile carbon dynamics (Ogle and Pacala, 2009).

We benchmarked the modules against representative observations and data from the literature (see SI, Section D). The key model outputs were internally consistent and reasonably in line with existing data for even-aged single-species forests (Fig. 3; SI, Fig. D.1), lending support to our model and results.

At stand level and averaged over the rotation, the carbon use efficiency (CUE), i.e., the complement to autotrophic respiration to gross primary productivity ratio, $(\mathrm{GPP} - R_a)/\mathrm{GPP}$, was comparable (0.49 and 0.32 for even-aged pine and spruce, respectively) with values observed for jack pine (0.34 to 0.43) and black spruce (0.29 to 0.39) respectively (Ryan et al., 1997, Table 7). Note that, in order to compare the CUE values with those in literature, we included foliage dark respiration during the day (R_d) in the denominator of the calculated CUE.

The modelled total tree biomass carbon for even-aged spruce ($6.7\,\mathrm{kgC\,m^{-2}}$) was within the range observed in 40 yr old forests across Sweden (between 4 and $8\,\mathrm{kgC\,m^{-2}}$; Berggren Kleja et al., 2007, Fig. 3a). The mean radial growth over 5 yr of both spruce and pine was in line with forest inventory data (Repola, 2009, Table 3), (SI, Fig. D.1). These reliable estimates of mean radial growth over 5 yr ensure that trunk volume growth is reasonably well simulated over time. Because dbh drives the tree allometry via the external statistical allometries (Lehtonen, 2005, Repola, 2009, Repola and Ahnlund Ulvcrona, 2014), accordance of modelled mean radial growth with observations lends support to the modelled biomass of the tree organs. The mean trunk wood densities ($481\,\mathrm{kg_{dw}\,m^{-3}}$ for even-aged pine and $385\,\mathrm{kg_{dw}\,m^{-3}}$ for even-aged spruce) were just outside the ranges emerging from tree inventories ($350 - 460\,\mathrm{kg_{dw}\,m^{-3}}$ and $390 - 410\,\mathrm{kg_{dw}\,m^{-3}}$ for pine and spruce forests, respectively; Repola 2006, Fig. 4). Deviations possibly arose from discrepan-

cies between literature values for wood density and wood density as derived from allometric relationships, in particular for small trees, and by averaging the wood density over several trees and the entire rotation. SI, Section D, provides more in-depth tests of the model's biomass predictions.

4.3. Implications for planning forest management for different goals

Managed forests need to provide biomass while increasingly supporting climate change mitigation efforts. These goals are often in contrast (Jandl et al., 2007b, Noormets et al., 2015, Jandl et al., 2007a), calling for robust approaches and metrics to evaluate benefits and drawbacks of different management strategies, in support of the scientific and public debate (Sierra et al., 2021). We developed a model that allows to evaluate both wood production and climate change mitigation potential of management alternatives at different timescales. To this aim, the model follows tree-, stand- and wood-product carbon dynamics and carbon flows from the initial photosynthetic uptake to the release back into the atmosphere (Fig. 1). We demonstrated the model capabilities by contrasting four management scenarios that represent idealized cases of typical management chains in the Nordic countries. The even-aged single/mixed-species stands mimic rotational forestry, while the mixed-aged scenario resembles continuous-cover management.

The results show that, despite the same starting point in terms of carbon stocks in trees, soil and wood products, management alternatives lead to different pathways of carbon stocks and climate change mitigation potential. Regarding net carbon sequestration, all even-aged scenarios yield more than the mixed-aged pine after an 80-yr rotation (ICNB, mixed: +31 %, pine: +29 %, spruce: +19 %; Fig. 4; Table 2). In terms of wood products, the mixed-aged and mixed-species scenarios were the most productive (Table 2). The high productivity of small-diameter wood in the mixed-aged and even-aged pine scenarios can support fossil-fuel substitution and climate change mitigation (Schulze et al., 2020). This is important, given that the current amount of logging residues in, e.g., Sweden might not suffice in the future

(Börjesson et al., 2017).

While wood production and carbon sequestration are relevant metrics for forest managers, they are insufficient to quantify the climate impacts of boreal forest management. For the latter, the time horizon considered, the fate of legacy carbon (i.e., the carbon initially in the system) and the retention effect of wood-product carbon are key, as apparent from the differing rankings of our sample management scenarios (Table 2 & Fig. 5). Thus, to evaluate the climate change mitigation potential, the metric ICS (integrated carbon stocks, including transit times and effects of legacy carbon) is necessary. The inclusion of retention effects of wood-product carbon into ICS increases the climate change mitigation potential of the mixed-aged scenario by +44 %, while the even-aged scenario (pine) with the most increasing climate change mitigation potential improves only by +28 %. Our estimated ICS suggests that all the even-aged scenarios are inferior to mixed-aged management, unless the planning horizon is extended to the end of the 80 yr-rotation. The rate at which the even-aged management scenarios regain their carbon sequestration and climate change mitigation potential after the clear-cut, compared with the mixed-aged stand (Fig. 5) or delayed set-a-side management (not considered), must be compared with the timescales of the climate targets. For instance, Finland aims at carbon neutrality by 2035 (Huttunen et al., 2022), but our model shows that the recovery from the initial loss of carbon storage due to clear-cut requires almost the entire 80-yr rotation to compensate for the lost climate change mitigation potential. Clear-cut management thus has significant negative effects on short-term ($\leq$ 50 yrs) climate goals (Fig. 5).

In addition to wood production, carbon sequestration and climate change mitigation potential, there are other factors (not included in the model) that generally favor mixed-aged and mixed-species forests Messier et al. (2022). Despite lacking an explicit facilitation effect in the model, the simulated species mixture yielded ca. 9 % more total wood products than a theoreti-

cal $50 - 50$ mix of mono-specific forests (Table 2). Such slight overyielding is expected (Ruiz-Peinado et al., 2021). We can also conclude that pine contributes slightly more than spruce to IITT in the mixed-species simulation (55 % compared with 45 %). In particular, during the first 50 yr the contribution of pine is much higher than the one of spruce, and later the relative contribution of spruce increases. However, we cannot disentangle the contributions of different species to INCB and ICS because we cannot attribute the effects of legacy carbon to a specific species. Moreover, more diverse forests are less susceptible to biotic and abiotic disturbances such as pest outbreaks (Jactel et al., 2021) and extreme weather events (Bauhus et al., 2017), thus increasing ecosystem stability (Loreau, 2022). Mixed-species forests also tend to harbor greater biodiversity (Ampoorter et al., 2020) and are also often more socially accepted (Ribe, 1989, Gundersen and Frivold, 2008). Upon availability of physiological parameters and allocation rules, inclusion of broadleaf species such as birch or other mixtures of three or more species in the simulations is possible. Also understory vegetation, currently neglected in the model, could contribute substantially to the stand carbon dynamics and fill spatial or functional niches.

5. Conclusions

We developed a forest-growth and carbon-balance model that combines process-based modules for gross-primary productivity as well as autotrophic and heterotrophic respiration with mass-conserving statistical carbon allocation in a tree. The model allows to track the age distribution of carbon in the tree-soil-wood product system, enabling the quantification of both wood production and climate change mitigation potential of different forest management scenarios across an entire rotation. The model was tested and its capabilities demonstrated for four idealized management scenarios resembling even-aged and continuous-cover forestry in Fennoscandia.

Over the 80 yr rotation, the wood production was highest in the mixed-

aged pine scenario for both short- and long-lasting wood products. Nevertheless, in terms of carbon sequestration, all even-aged scenarios were more effective than the mixed-aged strategy, although the even-aged scenarios show a clearly lower climate change mitigation potential for most of the rotation compared with the mixed-aged scenario. The inclusion of legacy carbon and wood-product retention effects emphasized the advantage of the mixed-aged pine scenario over clear-cut based scenarios. While even-aged scenarios were sequestering more carbon over the rotation cycle, the initial clear-cut effects on carbon stocks (INCB) were compensated only after about 42 to 45 yr. However, a transit-time based metric including the retention time of carbon from the atmosphere (ICS) shows that it takes almost a typical rotation of 80 yr (or longer) to compensate for the lost climate regulation caused by an initial clear cut.

These results clearly show that transit-time based climate change mitigation potential and pure carbon sequestration provide different information and hence ranks of management scenario performances. Further, it is necessary to consider also the fate of the legacy carbon and wood-products when addressing climate change mitigation potential of forestry. It is thus imperative to select the evaluation metrics based on the desired goal and clearly specify the timescales of interest when evaluating climate change mitigation potential of forest management.

Author contributions

Holger Metzler: methodology, software, validation, formal analysis, investigation, data curation, writing (original draft), visualization; **Samuli Launiainen:** software (photosynthesis module), validation, writing (review & editing), funding acquisition; **Giulia Vico:** conceptualization, validation, writing (review & editing), supervision, project administration, funding acquisition

Acknowledgements

Funding was provided by the Swedish Research Council for Sustainable Development FORMAS, under grant 2018-01820, and the Research Council of Finland (grant no. 348102). We thank Carlos A. Sierra, Henrik Hartmann, and David Herrera from Max Planck Institute for Biogeochemistry Jena, Germany, for fruitful discussions and input, and are particularly grateful to Carlos A. Sierra for providing access to computing facilities.

Supplementary Information

Part A Detailed model description

Photosynthetically fixed carbon enters the the *MeanTree*s as glucose and is distributed to the single trees represented by the *MeanTree*. Single tree carbon dynamics are based on ACGCA (Ogle and Pacala, 2009). The glucose carbon is allocated to tree organs as part of tissues (g_{dw}) and to labile storage (g_{gluc}). In order to describe single-tree carbon dynamics in units of gC, we need to convert g_{dw} and g_{gluc} to gC using the two conversion constants

$$\zeta_{dw} := 0.5\,\frac{\mathrm{gC}}{\mathrm{g_{dw}}} \quad \text{and} \quad \zeta_{gluc} := \frac{72}{180.15}\,\frac{\mathrm{gC}}{\mathrm{g_{gluc}}}. \tag{A.1}$$

On single-tree level, the carbon cycling is then described in units of gC and on *MeanTree* level, in the soil, and in wood products in units of $\mathrm{gC\,m^{-2}}$.

A.1 Photosynthesis module

The photosynthesis module computes gross-primary productivity (GPP_i) of each *MeanTree* at a half-hourly time step, and accumulates it to annual GPP_i for the tree module. It uses established approaches to compute needle level photosynthesis (Farquhar-model with co-limitation, (Farquhar et al., 1980, Launiainen et al., 2022)) and stomatal conductance (USO, (Medlyn et al., 2012)). The short-wave radiation, leaf gas-exchange and seasonal cycle sub-modules are adopted from the multi-layer APES-model (Launiainen et al., 2015, Leppä et al., 2020) (see summary of parameters in Table A.1). Rainfall and snow interception, snowpack dynamics and soil water balance (a bucket model) are based on the SpaFHy -model (Launiainen et al., 2019).

The forest stand consists of one or several *MeanTree*s, whose dimensions (height and leaf-area density distribution, LAD_i) are updated in the beginning of each year. The stand LAD is computed as the sum of LAD_is and determines radiation and wind attenuation in the canopy. The transmittance

and absorption of photosynthetically active radiation (PAR) and fraction of sunlit foliage at each canopy layer (here 30) are computed following Zhao and Qualls (2005), with adaptations to coniferous canopy described in Launiainen et al. (2015). The photosynthesis and transpiration rates are subsequently computed separately for sunlit and shaded needles of each *MeanTree* and canopy layer, assuming the leaves are at the air temperature. The leaf-level rates are then integrated over the leaf-area density and time to provide annual GPP_i and transpiration of each *MeanTree*.

The response of leaf gas-exchange to limited soil water availability is accounted for by decreasing the USO model parameter g_1 (proportional to inverse of marginal water use efficiency) and maximum carboxylation rate ($V_{cmax,25}$) at 25°C whenever relative plant available water (REW) is below a critical threshold. The non-linear response is formulated as $x = x_{ww} \times (\frac{REW}{b_0})^{b_1}$, where x_{ww} is the property ($g_1, V_{cmax,25}$ etc.) in well-watered conditions, and parameters b_i are fitted based on pine shoot gas-exchange data from Hyytiälä SMEAR II-site in Southern Finland. For details, see Launiainen et al. (2022, 2015). A standard approach is used for the temperature response of the Farquhar-model parameters (Medlyn et al., 2002, Kattge and Knorr, 2007), while the seasonal cycle of photosynthetic capacity is accounted for by making $V_{cmax,25}$ a function of delayed air temperature (Kolari et al., 2007). For details, see Supplementary material of Launiainen et al. (2015) and Launiainen et al. (2022).

The soil water content (θ) is solved with a two-layer bucket model (Launiainen et al., 2019). The top layer resembles organic litter/moss and acts as a rainfall interception storage, and the lower layer represents the plant root zone (here depth $D = 0.5\,\mathrm{m}$), whose hydraulic properties are described using Van Genuchten's (1980) approach. The snow accumulation and melt is modelled using the degree-day approach, and rainfall interception is computed assuming the canopy behaves as a single big leaf with one effective water storage. For details, see Launiainen et al. (2019).

The used needle gas-exchange, radiation and water balance sub-models have been tested independently and as part of the evaluation of a multi-layer ecosystem model (APES, Launiainen et al., 2015) against observed ecosystem level eddy-covariance-based carbon, water and energy fluxes at several boreal coniferous forests (Launiainen et al., 2015, Leppä et al., 2020). Moreover, the approach has shown to well reproduce the observed non-linear response of stand-level GPP and evapotranspiration (ET) to stand leaf-area index (LAI) across several boreal forest sites (Launiainen et al., 2015, 2016).

For this work, we further tested that our simplified vertically-resolved model, omitting the air temperature and humidity gradients within the canopy simulated by APES, predicted the expected non-linear response of ecosystem GPP and ET to LAI. We also compared simulated annual GPP and its inter-annual variability with the long-term time-series from Hyytiälä coniferous forest in Southern Finland (Launiainen et al., 2022) with satisfactory results (not shown). The benchmarking lends support that the *MeanTree*'s annual GPP_i and its dependency on stand structure, i.e., light competition via stand LAD and *MeanTree* LAD profiles, and weather conditions are adequately described.

Parameter	**Value**	**Description**
$V_{cmax,25}$	60 (pine), 50 (spruce) molm-2s^{-1}	maximum carboxylation rate at 25°C
$J_{max,25}$	1.97× $V_{cmax,25}$	maximum electron transport rate at 25°C, Kattge and Knorr (2007)
$R_{d,25}$	0.5 molm^{-2}s^{-1}	dark respiration rate at 25°C
α	0.3 (-)	quantum efficiency parameter, Launiainen et al. (2022)
θ	0.7 (-)	curvature parameter
β	0.95 (-)	co-limitation parameter
g_1	2.6 kPa$^{0.5}$	USO model parameter, Launiainen et al. (2015), Leppä et al. (2020)
g_0	0.001 molm^{-2}s^{-1}	USO model, residual conductance for H_2O, Launiainen et al. (2015)
$a_0,\ a_1$	0.39, 0.83	g_1 response to plant available water, Launiainen et al. (2022)
$b_0,\ b_1$	0.39, 0.83	$V_{cmax,25}$ response to plant available water, Launiainen et al. (2022)
α_p	0.1 (-)	shoot and ground PAR albedo, Launiainen et al. (2015)
f_{clump}	0.7 (-)	foliage clumping factor, (Launiainen et al., 2015)
W_{max}	0.2 kg H_2O LAI^{-1}	canopy interception storage, Launiainen et al. (2019)
D	0.5 m	root zone depth
θ_s	0.50 m^{3}m^{-3}	porosity
θ_r	0.03 m^{3}m^{-3}	residual water content
α_s	0.06 m^{-1}	air-entry potential
n	1.35 (-)	pore size distribution parameter

Table A.1: Photosynthesis and water balance model parameters.

A.2 Tree module

The tree module represents the dynamics of carbon stocks (in units of grams of carbon, gC) within each single tree represented by a *MeanTree*. The *MeanTree* i represents N_i identical single trees per ground area and we consider the stocks per *MeanTree* in units of $\mathrm{gC\,m^{-2}}$.

Each tree's transient pool E receives GPP_i (gC) based on the previous year's photosynthesis. Part of this leaves E to the atmosphere as maintenance respiration $R_M = M_L + M_R + M_S$, consisting of leaf maintenance (M_L), fine root maintenance (M_R) and sapwood maintenance (M_S) costs. Sapwood maintenance M_S is combined for coarse roots and branches ("other") and the trunk.

The remaining carbon, $C_{\mathrm{alloc}}\,\Delta t = E - R_M\,\Delta t$, with $\Delta t = 1\,\mathrm{yr}$, becomes available for allocation to tree organs, according to the rules specified below. The carbon allocated to the tree organs is subsequently used for sapwood transformation to heartwood ("other" and trunk), for growth of tissues (including replacement of tissue turnover and growth of new tissue), growth respiration, and for labile carbon associated to newly created tissue. The labile carbon (C_L, C_R, C_S) associated to tissue lost due to senescence returns to the transient pool E. Labile carbon (C_S) associated to sapwood (B_{TS}, B_{OS}) that is transformed to heartwood (B_{TH}, B_{OH}) is incorporated into the heartwood.

The following sections describe the external and internal fluxes of different tree organs (leaves, fine roots, coarse roots and branches, trunk). Planting a tree introduces carbon to the forest stand that is part of a new tree as external input flux, and fluxes caused by forest harvesting are described in SI, Section A.5.

A.2.1 Leaves and fine roots

A schematic for the leaf pools and fluxes is shown in Fig. A.1. The carbon dynamics in fine roots is analogous. The external input flux to the transient

pool is indicated by $\searrow$, external output fluxes by $\nearrow$, and fluxes between pools inside the model by $\rightarrow$.

Leaf maintenance respiration is given by

$$M_L = R_{\mathrm{mL}}\, B_L\, \frac{\zeta_{\mathrm{gluc}}}{\zeta_{\mathrm{dw}}}, \tag{A.2}$$

where R_{mL} is the species-specific leaf maintenance respiration rate ($\mathrm{g_{gluc}\, g_{dw}^{-1}\, yr^{-1}}$).

The fraction f_L of $C_{\mathrm{alloc}}\,\Delta t$ is allocated to leaves and split in three components: leaf tissue growth (B_L), transfer into the leaf labile storage pool (C_L), and growth respiration (G_L). Leaf tissue construction comes at costs C_{gL} ($\mathrm{g_{gluc}\, g_{dw}^{-1}}$) and induces growth respiration

$$G_L = \frac{C_{\mathrm{gL}}}{C_{\mathrm{gL}} + \delta_L}\,(1-\eta_L)\, f_L\, C_{\mathrm{alloc}}\,\Delta t, \tag{A.3}$$

where

$$\eta_L = \frac{1}{C_{\mathrm{gL}}}\,\frac{\zeta_{\mathrm{dw}}}{\zeta_{\mathrm{gluc}}} \tag{A.4}$$

is the carbon use efficiency during leaf tissue growth (regrowth and net growth). Allocation to leaf tissue (B_L), including regrowth of senescent tissues and net growth (net biomass increase), and associated labile storage (C_L) are balanced such that the ratio of labile storage to leaf structural biomass carbon remains constant (δ_L, $\mathrm{g_{gluc}\, g_{dw}^{-1}}$).

Leaf tissue is lost due to senescence at a species-specific senescence rate S_L ($\mathrm{yr^{-1}}$), generating a loss ($S_L\, B_L$). The labile storage carbon ($S_L\, C_L$) associated to this tissue loss returns to the tree's common transient pool (E).

A.2.2 Trunk

A schematic for the trunk component is shown in Fig. A.2. The trunk consists of the tissue pools B_{TS} and B_{TH} and shares one labile storage pool (C_S) with coarse roots and branches ("other‘"). Carbon allocated to the trunk

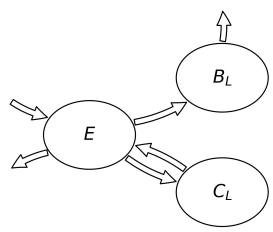

Figure A.1: Leaf carbon stocks and fluxes.

External input fluxes

- $\searrow E$: GPP

External output fluxes

- $E \nearrow$: $M_L + G_L$

Internal fluxes

- $E \to B_L$: $f_L \cdot \frac{C_{\mathrm{gL}}}{C_{\mathrm{gL}}+\delta_L} \cdot \eta_L \cdot C_{\mathrm{alloc}}$
- $E \to C_L$: $f_L \cdot \frac{\delta_L}{C_{\mathrm{gL}}+\delta_L} \cdot C_{\mathrm{alloc}}$
- $C_L \to E$: $S_L \cdot C_L$
- $B_L \to$ Litter: $S_L \cdot B_L$

comes from the transient pool E. The combined maintenance respiration of trunk sapwood and "other" sapwood is given by

$$M_S = R_{\mathrm{mS}} \cdot B_S^* \, \zeta_{\mathrm{gluc}}. \tag{A.5}$$

Here R_{mS} is the species-specific sapwood maintenance respiration rate ($\mathrm{g_{gluc}\, g_{dw}^{-1}\, yr^{-1}}$) and B_S^* is the biomass of living sapwood in $\mathrm{g_{dw}}$ (Ogle and Pacala, 2009, SI, Eq. (29)).

The amount $f_T \, C_{\mathrm{alloc}} \, \Delta t$ is allocated to the trunk and is split up in three components: sapwood growth (B_{TS}), transfer into the labile storage pool (C_S), and growth respiration (G_{TS}). Trunk sapwood construction from transient pool carbon comes at costs C_{gW} ($\mathrm{g_{gluc}\, g_{dw}^{-1}}$) and induces growth respiration

$$G_{\mathrm{TS}} = \frac{C_{\mathrm{gW}}}{C_{\mathrm{gW}} + \delta_W} \, (1 - \eta_W) \, f_T \, C_{\mathrm{alloc}} \, \Delta t. \tag{A.6}$$

Trunk tissue is not lost due to senescence.

Depending on heartwood volume growth (ΔB_{TH}), a fraction of trunk

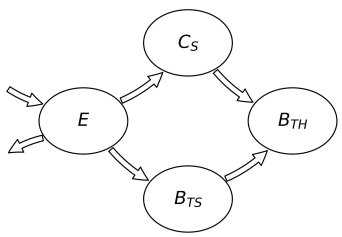

Figure A.2: Trunk carbon stocks and fluxes.

External input fluxes

- $\searrow E$: GPP

External output fluxes

- $E \nearrow$: $M_S + G_{\mathrm{TS}}$

Internal fluxes

- $E \to B_{\mathrm{TS}}$: $f_T \cdot \frac{C_{\mathrm{gW}}}{C_{\mathrm{gW}}+\delta_W} \cdot \eta_W \cdot C_{\mathrm{alloc}}$
- $E \to C_S$: $f_T \cdot \frac{\delta_W}{C_{\mathrm{gW}}+\delta_W} \cdot C_{\mathrm{alloc}}$
- $B_{\mathrm{TS}} \to B_{\mathrm{TH}}$: $v_T \cdot B_{\mathrm{TS}}$
- $C_S \to B_{\mathrm{TH}}$: $v_T \cdot \eta_{HW} \cdot \frac{B_{\mathrm{TS}}}{B_S} \cdot C_S$

sapwood ($v_T\, B_{\mathrm{TS}}$) is converted to heartwood with heartwood construction rate v_T given by Eq. (A.29). The associated labile storage ($v_T\, C_S\, B_{\mathrm{TS}}/B_S$, $B_S = B_{\mathrm{OS}} + B_{\mathrm{TS}}$), is directly incorporated into heartwood biomass at no costs. If the tree is in "static" or "shrinking" state, then no new heartwood is being constructed, i.e., $v_T = 0$.

A.2.3 Coarse roots and branches ("other")

A schematic for the coarse roots and branches ("other") component is shown in Fig. A.3. This tree component consists of the tissue pools B_{OS} and B_{OH}, while it shares the labile storage pool (C_S) with the trunk. As for other organs, the carbon allocated to the coarse roots and branches comes from the transient pool E. The combined maintenance respiration of trunk sapwood and "other" sapwood is given by Eq. (A.5).

The amount $f_O\, C_{\mathrm{alloc}}, \Delta t$ of C is allocated to coarse roots and branches and is split up in three components: sapwood growth (B_{OS}), transfer into the labile storage pool (C_S), and growth respiration ($G_{\mathrm{OS},E}$). Sapwood con-

struction comes at costs C_{gW} ($\mathrm{g_{gluc}\,g_{dw}^{-1}}$) and induces growth respiration

$$G_{\mathrm{OS},E} = \frac{C_{\mathrm{gW}}}{C_{\mathrm{gW}} + \delta_W}\,(1-\eta_W)\,f_O\,C_{\mathrm{alloc}}\,\Delta t, \tag{A.7}$$

where

$$\eta_W = \frac{1}{C_{\mathrm{gW}}}\,\frac{\zeta_{\mathrm{dw}}}{\zeta_{\mathrm{gluc}}} \tag{A.8}$$

is the carbon use efficiency during sapwood tissue production, and δ_W is the maximum labile storage capacity of newly produced sapwood.

In contrast to the trunk, coarse roots and branches are lost due to senescence. This senescence provides input to the coarse woody debris pool (CWD) of the soil module and concerns both sapwood ($S_O\,B_{\mathrm{OS}}$) and heartwood ($S_O\,B_{\mathrm{OH}}$), where S_O (yr^{-1}) is the species-specific senescence rate. The labile storage carbon associated to sapwood lost by senescence, $S_O\,C_S\,B_{\mathrm{OS}}/B_S$, returns to the transient pool E. Heartwood loss needs to be regrown from sapwood (including the associated labile storage from C_S), and the induced sapwood loss needs to be regrown from carbon coming from the transient pool E, considering growth costs and associated labile storage to C_S. The rate v_O of sapwood conversion to heartwood is determined such that heartwood losses are compensated and the tree meets the external statistically derived allometries (Eq. (A.43)). The labile storage carbon ($v_O\,C_S\,B_{\mathrm{OS}}/B_S$) associated to sapwood converted to heartwood is directly incorporated into heartwood biomass with efficiency $\eta_{\mathrm{HW}} = 1$. If the tree is in "static" or "shrinking" state, then the newly constructed sapwood biomass based on the available transient carbon is not sufficient to make up for senescence losses and heartwood production from sapwood. The missing amount of carbon to keep sapwood biomass unchanged is supplied by the labile pool C_S and given by $f_{C_S}\,C_S$ as described in Eq. (A.44). The flux $f_{C_S}\,C_S$ also induces growth respiration, which is given by

$$G_{\mathrm{OS},C_S} = f_{C_S}\,(1-\eta_W)\,C_S. \tag{A.9}$$

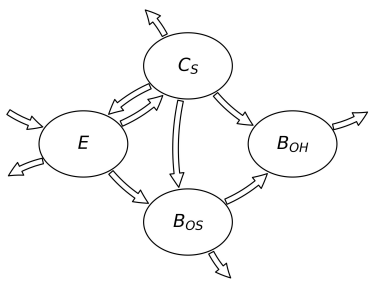

Figure A.3: Coarse root and branch carbon stocks and fluxes.

External input fluxes

- $\searrow E$: GPP

External output fluxes

- $E \nearrow$: $M_S + G_{\mathrm{OS},E}$
- $C_S \nearrow$: G_{OS,C_S}

Internal fluxes

- $E \to B_{\mathrm{OS}}$: $f_O \cdot \frac{C_{\mathrm{gW}}}{C_{\mathrm{gW}}+\delta_W} \cdot \eta_W \cdot C_{\mathrm{alloc}}$
- $E \to C_S$: $f_O \cdot \frac{\delta_W}{C_{\mathrm{gW}}+\delta_W} \cdot C_{\mathrm{alloc}}$
- $C_S \to E$: $S_O \cdot \frac{B_{\mathrm{OS}}}{B_S} \cdot C_S$
- $C_S \to B_{\mathrm{OS}}$: $f_{C_S} \cdot \eta_W \cdot C_S$
- $B_{\mathrm{OS}} \to B_{\mathrm{OH}}$: $v_O \cdot B_{\mathrm{OS}}$
- $C_S \to B_{\mathrm{OH}}$: $v_O \cdot \eta_{\mathrm{HW}} \cdot \frac{B_{\mathrm{OS}}}{B_S} \cdot C_S$
- $B_{\mathrm{OS}} \to$ CWD: $S_O \cdot B_{\mathrm{OS}}$
- $B_{\mathrm{OH}} \to$ CWD: $S_O \cdot B_{\mathrm{OH}}$

In contrast to sapwood construction by carbon coming from the transient pool E, sapwood construction from the labile storage pool C_S does not lead to additional storage in labile carbon associated to the newly produced sapwood, as the supplied carbon already comes from the labile pool. This allows a depletion of the labile storage.

A.3 Carbon allocation in the tree

A.3.1 Tree allometric relationships

All tree allometry rules are based on the *MeanTree*'s diameter at breast height (dbh, cm) and some additionally on the *MeanTree*'s height (H, m).

Tree height is computed as

$$H = 1.3 + \frac{\mathrm{dbh}^k}{(a + b\,\mathrm{dbh})^k} \tag{A.10}$$

based on the Näslund height model (Näslund, 1936) parameterized for 155 stands in southern Finland (Siipilehto, 2000). Since dynamic radial growth is (internally) computed at the *MeanTree*'s radius at trunk base (r, m), it is necessary to compute r from dbh and H. The computation of r differs between small and larger trees. For dbh < 3.0 cm, Laasasenaho (1982) suggests the diameter at trunk base to be

$$r = 2 + 1.25\,\frac{\mathrm{dbh}}{200}. \tag{A.11}$$

For dbh ≥ 3.0 cm, we use the tree radius at breast height ($r_{\mathrm{BH}} = 1/2\,\mathrm{dbh}$) to identify r through the current trunk-shape based relation as expressed in Ogle and Pacala (2009, SI, Eq. (24)).

We describe the allometrically derived biomass of leaves (m_L), stem wood (m_{SW}), stem bark (m_{SB}), living branches (m_{LB}), stump (m_S), and (coarse) roots (m_{CR}) in $\mathrm{kg_{dw}}$ based on the *MeanTree*'s diameter at breast height (dbh, cm) and its height (H, m) via the empirical relations based on tree inventory data. The allometric equations for leaves, stem wood, stem bark, living branches, stump and (coarse) roots for large trees come from Repola (2009). Trees are considered large if their dbh is at least the critical value, which is defined as mean dbh minus one standard deviation of the forest inventory data used to derive the allometric relationships. According to Repola (2009, Table 3) pines are considered large if dbh $\geq (13.1 - 5.3)$ cm and spruces if dbh $\geq (11.2 - 4.0)$ cm.

The allometric equations have the general form

$$\ln m_Y = \mathrm{intercept} + b_1\,\frac{\mathrm{dbh}}{\mathrm{dbh} + n} + b_2\,\frac{H}{H + m} + b_3\,\log(H) + b_4\,H, \tag{A.12}$$

where the b_is are empirical coefficients depending on the type of biomass Y, and a variance-correction term is added to the intercept to correct for the bias due to the logarithmic transformation:

$$\text{intercept} = b_0 + \frac{1}{2}\,(\sigma_u^2 + \sigma_e^2). \tag{A.13}$$

For small trees, the coefficients in Eq. (A.12) for stem wood and living branches were taken from Repola and Ahnlund Ulvcrona (2014). Empirical coefficients were not reported for stem bark, stump, and (coarse) roots of small trees. So we use the according coefficients for large trees here. The biomass equation for leaves in small trees is given by

$$m_L = a\,\mathrm{dbh}^b\,H^c \tag{A.14}$$

with coefficients for pine and spruce provided in Lehtonen (2005, Table 4).

The vertical distribution of leaf biomass in the crown follows Tahvanainen and Forss (2008, Table 8), based on the tree' crown base heights which derived from Tahvanainen and Forss (2008, Fig. 4).

To ensure continuity, the biomass curves of small trees are scaled such that they match the biomass curves of taller trees at the critical dbh. .

A.3.2 Routines for carbon allocation within a single tree

Each year we identify a new $\mathrm{dbh}^* = \mathrm{dbh}(t + \Delta t)$ so that the tree organs' new biomasses match the external allometric constraints as defined by dbh^* and Eq. A.12. Identifying dbh^* requires writing a carbon balance for each tree organ, i.e., for leaves (SI, Section A.3.3), for fine roots (SI, Section A.3.4), for the trunk (SI, Section A.3.5), and for coarse roots and branches (SI, Section A.3.6). The allocation fractions f_X (yr^{-1}) across organs must satisfy

$$f_L + f_R + f_T + f_O = 1\,\mathrm{yr}^{-1}, \tag{A.15}$$

where f_X is the fraction of the newly available carbon ($C_{\text{alloc}}\,\Delta t$) allocated to tree organ X. The new diameter at breast height (dbh*) appears in each f_X, via the relations linking the change in biomass of X to the fluxes in and out X, which are described next for each organ. The according species-dependent parameter values are shown in Tables A.3 and A.4. When the newly fixed carbon is insufficient to meet the demands imposed by replacement of biomass losses via senescence, the tree reverts to the "static" or "shrinking" state (SI, Section A.4.

A.3.3 Leaves

Each year, new carbon allocated from $C_{\text{alloc}}\,\Delta t$ to leaves is required for net growth of new leaf biomass (ΔB_L), to balance leaf biomass lost via senescence ($S_L\,B_L\,\Delta t$), for tissue growth costs (C_{gL}) and a fixed share of associated labile storage (δ_L) Ogle and Pacala (2009, SI, Eq. (1A)). Hence,

$$f_L\,C_{\text{alloc}}\,\Delta t = (\Delta B_L + S_L\,B_L\,\Delta t)\,(C_{\text{gL}} + \delta_L)\,\frac{\zeta_{\text{gluc}}}{\zeta_{\text{dw}}}, \tag{A.16}$$

where both sides of the equation are in gC. The dependence of f_L on dbh* comes through its dependence on the net biomass growth

$$\Delta B_L = B_L^* - B_L = B_L(\text{dbh}^*) - B_L. \tag{A.17}$$

We assume that labile carbon associated to leaves (C_L) is actually stored within the leaves. Hence, we require the new leaf biomass carbon and labile pool to equal the leaf biomass carbon imposed by the allometric relationship (Eq. (A.12)). In formulas,

$$B_L^* + C_L^* = 10^3 m_L^*\,\zeta_{\text{dw}}, \tag{A.18}$$

where $m_L^* := m_L(\text{dbh}^*, H^*)$ is the biomass from the allometric model (Eq. (A.12)) applied to leaves (in g_{dw}), and ζ_{dw} transforms g_{dw} into gC. C_L is calculated as a fraction of the biomass carbon itself, as $C_L^* = \delta_L\,B_L^*\,\zeta_{\text{gluc}}\,\zeta_{\text{dw}}^{-1}$. By rear-

ranging the terms, we obtain

$$B_L^* = \frac{10^3\, m_L^*}{1 + \delta_L\, \frac{\zeta_{\mathrm{gluc}}}{\zeta_{\mathrm{dw}}}}\, \zeta_{\mathrm{dw}}. \tag{A.19}$$

A.3.4 Fine roots

Similarly to leaves, the fine root fraction is given by (Ogle and Pacala, 2009, SI, Eq. (1B)),

$$f_R\, C_{\mathrm{alloc}}\, \Delta t = (\Delta B_R + S_R\, B_R\, \Delta t)\, (C_{\mathrm{gR}} + \delta_L)\, \frac{\zeta_{\mathrm{gluc}}}{\zeta_{\mathrm{dw}}}. \tag{A.20}$$

The new fine root biomass is computed as a constant fraction of the new leaf biomass, $B_R^* = \rho_{\mathrm{RL}}\, B_L^*$.

A.3.5 Trunk

Carbon allocated to the trunk is used for net sapwood growth ($\rho_W\, \Delta V_T$) involving sapwood construction costs (C_{gW}) and a labile storage fraction (δ_W). The formula given by Ogle and Pacala (2009, SI, Eq. (31C)),

$$f_T\, C_{\mathrm{alloc}}\, \Delta t = \left(\rho_W\, \Delta V_T\, \zeta_{\mathrm{dw}} - \frac{\delta_S}{C_{\mathrm{gHW}}}\, v_T\, B_{\mathrm{TS}}\, \Delta t\right) \cdot (C_{\mathrm{gW}} + \delta_W)\, \frac{\zeta_{\mathrm{gluc}}}{\zeta_{\mathrm{dw}}}, \tag{A.21}$$

allows ρ_W to become negative for slowly growing trunk volumes. Furthermore, we assume labile carbon associated to the trunk to be part of the trunk volume. Consequently, we adapt this formula and compute f_T from

$$f_T\, C_{\mathrm{alloc}}\, \Delta t = \rho_W\, \Delta V_T\, \zeta_{\mathrm{dw}}\, \cdot (C_{\mathrm{gW}} + \delta_W)\, \frac{\zeta_{\mathrm{gluc}}}{\zeta_{\mathrm{dw}}}. \tag{A.22}$$

Because of sapwood transformation to heartwood ($v_T\, B_{\mathrm{TS}}\, \Delta t$) with unitary efficiency ($C_{\mathrm{gHW}} = 1.00\, \mathrm{g_{gluc}\, g_{dw}^{-1}}$), the labile storage fraction

$$\delta_S := \frac{C_S}{B_S}\, \frac{\zeta_{\mathrm{dw}}}{\zeta_{\mathrm{gluc}}} \text{ with } B_S := B_{\mathrm{TS}} + B_{\mathrm{OS}} \tag{A.23}$$

associated to transformed sapwood becomes becomes integrated into heartwood.

Once f_T is identified, according to Ogle and Pacala (2009, SI, Eqs. (1C) and (1D)), we determine

$$\Delta B_{\mathrm{TS}} = \frac{f_T\, C_{\mathrm{alloc}}\, \Delta t}{C_{\mathrm{gW}} + \delta_W} - v_T\, B_{\mathrm{TS}}\, \Delta t \tag{A.24}$$

and

$$\Delta B_{\mathrm{TH}} = \left(1 + \frac{\delta_S}{C_{\mathrm{gHW}}}\right) v_T\, B_{\mathrm{TS}}\, \Delta t. \tag{A.25}$$

In order to determine f_T from Eq. (A.22), we need to identify the density of newly produced sapwood (ρ_W), the sapwood to heartwood conversion rate of the trunk (v_T), and the maximum labile carbon storage capacity of newly produced sapwood (δ_W). Since δ_W depends on ρ_W, and both ρ_W and v_T depend on the new heartwood volume $V^*_{\mathrm{TH}} = V_{\mathrm{TH}}(dbh^*, \mathrm{SW}^*))$, which in turn depends on the new sapwood width $\mathrm{SW}^* = \mathrm{SW}(\mathrm{dbh}^*)$, we first describe how to identify SW^* and then how we derive V^*_{TH} from it. The density of newly produced sapwood $\rho_W = \rho_W(\mathrm{dbh}^*)$ is then dynamically chosen such that the modelled trunk biomass follows the external allometries.

Sapwood width. We compute SW^* (m) such that the ratio of sapwood to heartwood width (HW^*, m) follows Sellin (1994). From Eq. [2] we get

$$\mathrm{SW}_{\mathrm{Sellin}} = \frac{\mathrm{SW}_a\, d^*}{d^* + \mathrm{SW}_d} \tag{A.26}$$

in cm and from Fig. 1 we get

$$\mathrm{HW}_{\mathrm{Sellin}} = \mathrm{HW}_{\mathrm{slope}}\, d^*, \tag{A.27}$$

where $d^* = 200\, r^*$ is the new diameter at trunk base in cm. Then we obtain

$$\mathrm{SW}^* = \frac{\mathrm{SW}_{\mathrm{Sellin}}}{\mathrm{SW}_{\mathrm{Sellin}} + \mathrm{HW}_{\mathrm{Sellin}}}\, r^*. \tag{A.28}$$

Trunk heartwood volume. The new trunk heartwood volume V^*_{TH} in m^3 is computed as in Ogle and Pacala (2009, SI, Eq. (14)) with a mathematical correction of the formula for heartwood height (SI, Eq. (13)).

Sapwood to heartwood conversion rate of trunk. The sapwood to heartwood conversion rate of the trunk, $v_T = v_T(V^*_{\mathrm{TH}})$ in yr^{-1}, is given as in Ogle and Pacala (2009, SI, Eq. (2)) by

$$v_T = \frac{\Delta V_{\mathrm{TH}}}{V_{\mathrm{TS}}\,\Delta t}, \tag{A.29}$$

where $\Delta V_{\mathrm{TH}} = V^*_{\mathrm{TH}} - V_{\mathrm{TH}}$. The trunk sapwood volume is denoted by $V_{\mathrm{TS}} = V_T - V_{\mathrm{TH}}$, and the trunk volume $V_T = V_T(\mathrm{dbh})$ is given by Ogle and Pacala (2009, SI, Eq. (9)).

Density of newly produced sapwood. While sapwood converted to heartwood does not change the trunk volume, new sapwood is needed for radial trunk growth. The allometrically derived trunk biomass is given by

$$m_T := m_{\mathrm{SW}} + m_{\mathrm{SB}} + m_S, \tag{A.30}$$

consisting of stem wood, stem bark, and the stump as given by Eq. (A.12). The trunk biomass carbon is given by

$$B_T = B_{\mathrm{TH}} + B_{\mathrm{TS}} + \frac{B_{\mathrm{TS}}}{B_S}\,C_S, \tag{A.31}$$

assuming that labile carbon associated to trunk sapwood is actually stored in the trunk. In order to match the allometrically derived trunk biomass by modelled biomass, we strive for $B^*_T = m^*_T$, which leads to the goal of

$$\Delta B_T = m^*_T - B_T. \tag{A.32}$$

Considering growth costs, we have

$$\Delta B_T = f_T\, C_{\text{alloc}}\, \Delta t\, \frac{1+\delta_W}{C_{\text{gW}}+\delta_W}. \tag{A.33}$$

We combine Eq. (A.33) with Eq. (A.22), and obtain ρ_W from

$$\rho_W = \frac{m_T^* - B_T}{\Delta V_T\,(1-\delta_W)} \tag{A.34}$$

under the additional conditions that

$$\rho_{W_{\text{min}}} \leq \rho_W \leq \rho_{W_{\text{max}}}. \tag{A.35}$$

Maximum labile carbon storage capacity of newly produced sapwood. We compute the maximum labile carbon storage capacity of newly produced sapwood as in Ogle and Pacala (2009, SI, Eq. (6)) by

$$\delta_W = \frac{\gamma_C\,(1-\gamma_X-\gamma_W\,\rho_W)}{\rho_W}. \tag{A.36}$$

A.3.6 Coarse roots and branches ("other")

Carbon allocated to "other" is needed for net sapwood biomass growth (ΔB_{OS}) and to balance losses of sapwood to senescence ($S_O\, B_{\text{OS}}\, \Delta t$) and to heartwood production ($v_O\, B_{\text{OS}}\, \Delta t$). For each term, there are sapwood construction costs (C_{gW}) and an associated labile storage fraction (δ_W) involved. Hence, following Ogle and Pacala (2009, SI, Eq. (1E)),

$$f_O\, C_{\text{alloc}}\, \Delta t = [\Delta B_{\text{OS}} + (S_O + v_O)\, B_{\text{OS}}\, \Delta t] \cdot (C_{\text{gW}} + \delta_W)\, \frac{\zeta_{\text{gluc}}}{\zeta_{\text{dw}}}. \tag{A.37}$$

In order to determine f_O from Eq. (A.37), we need to identify the net sapwood biomass carbon change ($\Delta\, B_{\text{OS}}$) and the sapwood to heartwood conversion rate of "other" (v_O). First, we compute $\Delta\, B_{\text{OS}}$, then we compute the net heartwood biomass carbon change of "other" (ΔB_{OH}) and use it to identify

v_O.

Net sapwood biomass carbon change of "other". The new sapwood biomass carbon of "other" (B^*_{OS}) is allometrically defined as

$$B^*_{\mathrm{OS}} = \lambda^*_S \cdot B^*_{\mathrm{TS}}, \tag{A.38}$$

where

$$\lambda^*_S = \frac{m^*_O}{m^*_T} \tag{A.39}$$

is the ratio of "other" biomass to trunk biomass as derived from external allometries. Allometric "other" biomass is computed as the sum of biomasses of living branches and (coarse) roots in Eq. (A.12), i.e.,

$$m_O := m_{\mathrm{LB}} + m_{\mathrm{CR}}. \tag{A.40}$$

Obviously, $\Delta B_{\mathrm{OS}} = B^*_{\mathrm{OS}} - B_{\mathrm{OS}}$.

Heartwood biomass carbon change of "other". The new heartwood biomass carbon of "other" (B^*_{OH}) is allometrically defined as

$$B^*_{\mathrm{OH}} = \lambda^*_H \cdot B^*_{\mathrm{TH}}, \tag{A.41}$$

where

$$\lambda^*_H = \lambda^*_S = \frac{m^*_O}{m^*_T} \tag{A.42}$$

is the ratio of "other" biomass to trunk biomass as derived from external allometries. Obviously, $\Delta B_{\mathrm{OH}} = B^*_{\mathrm{OH}} - B_{\mathrm{OH}}$.

Sapwood to heartwood conversion rate of "other". Heartwood production must satisfy net heartwood biomass growth (ΔB_{OH}) and make up for senescence losses ($S_O\, B_{\mathrm{OH}}\, \Delta t$), while carbon supply is provided by the sapwood pool ($v_O\, B_{\mathrm{OS}}\, \Delta t$) and by the labile storage pool ($v_O\, \delta_S\, B_{\mathrm{OS}}\, \Delta t$) at no heartwood construction costs ($C_{\mathrm{gHW}} = 1.00\, \mathrm{g_{gluc}\, g_{dw}^{-1}}$). Consequently, following

(Ogle and Pacala, 2009, SI, Eq. (1F)),

$$v_O \left(1 + \frac{\delta_S}{C_{\mathrm{gHW}}}\right) B_{\mathrm{OS}}\, \Delta t = \Delta B_{\mathrm{OH}} + S_O\, B_{\mathrm{OH}}\, \Delta t. \tag{A.43}$$

A.4 Physiological tree states

In case a *MeanTree* is subject to excessive competition for light and its annual photosynthetic carbon uptake is insufficient to sustain maintenance respiration and biomass regrowth caused by senescence in leaves, fine roots, and coarse roots and branches ("other"), the *MeanTree* changes its physiological status from "healthy" to "static". In the "static" state, the *MeanTree* has no radial trunk growth but only regrows the senescent biomass in leaves and fine roots from $C_{\mathrm{alloc}}\, \Delta\, t$. The amount of carbon insufficient to regrow all lost sapwood and heartwood "other" is extracted from the labile storage pool (C_S) and can be computed by

$$\begin{aligned} f_{C_S}\, C_S = {} & (S_O + v_O)\, B_{\mathrm{OS}}\, \Delta t\, C_{\mathrm{gW}}\, \frac{\zeta_{\mathrm{gluc}}}{\zeta_{\mathrm{dw}}} \\ & - C_{\mathrm{alloc}}\, \Delta t\, (1 - f_L - f_R)\, \frac{C_{\mathrm{gW}}}{C_{\mathrm{gW}} + \delta_W}. \end{aligned} \tag{A.44}$$

In "healthy" trees, $f_{C_S} = 0\,\mathrm{yr}^{-1}$. The first part of the right hand side is the hypothetical amount of carbon required for sapwood regrowth at costs C_{gW} because of senescence and heartwood construction if all carbon for that came from C_S. Recall that, other than from $C_{\mathrm{alloc}}\, \Delta t$, sapwood construction from C_S does not involve an additional share (δ_W) to be stored in labile carbon (C_S). Some carbon included in the first part of the right hand side, however, is already provided by $C_{\mathrm{alloc}}\, \Delta t$ and is represented by the second part of the right hand side. This amount does not need to be provided by C_S. By using $f_{C_S}\, C_S$ from the labile storage pool, $\Delta B_{\mathrm{OH}} = \Delta B_{\mathrm{OS}} = 0$ and the tree can potentially survive in the "static" state for a few years after which the light situation might improve and allow the tree to return to the "healthy" state. Labile storage carbon from C_S cannot be used for regrowth of leaves and fine

root biomass.

If $C_{\text{alloc}}\,\Delta t$ is not even enough to regrow senescence losses from leaves and fine roots only, then the tree switches to the "shrinking" state. In this state, leaves, fine roots, and "other" receive carbon from photosynthesis proportional to their respective demand in the "healthy" state for regrowth such that all captured carbon is used up. This means that the *MeanTree* loses biomass of leaves and fine roots, while the biomass in coarse roots and branches is regrown with the support from labile storage in C_S. When C_S becomes empty, the *MeanTree* dies and is removed from the stand. However, if before death the light situation improves, the *MeanTree* switches back to the "healthy" physiological state with no delay.

A.5 Carbon transfers via thinning and cutting and short- and long-lasting wood products

When a *MeanTree* in a stand is subject to thinning (partial removal) or cutting (complete removal), some tree carbon is transferred to the soil and wood products. Wood products with two different mean life times are considered: pulpwood or bioenergy (WP_S), represented via a short-lasting pool with fast turnover rate ($0.3\,\text{yr}^{-1}$); and long-lasting wood products (WP_L), represented by a pool with slow turnover rate ($0.02, \text{yr}^{-1}$). At the end of the wood product's lifetime, carbon returns from the wood-product module to the atmosphere as CO_2 emission. The turnover rates are taken from Pukkala (2014, Table 4).

The allocation of carbon from trees to soil and wood products depends on the tree's species and size and hence its stem shape (taper curve) (Laasasenaho, 1982, Eq. (33.1), parameters (41.1)). The stem is partitioned into saw log, fibre and cutting residues depending on stem dimensions. We set the minimum diameter and length for saw logs as 16.0 cm and 4 m, respectively, while the minimum dimensions for fibre wood are 8 cm in diameter and 3 m in length. The lowest 0.2 m of the stem is considered as stump.

The carbon in saw logs is considered as long-lasting wood product and is transferred to WP_L, while fibre is considered a short-lasting wood product and is transferred to WP_S. All other material (residue, stump) from "other" and the trunk is transferred to the CWD pool in the soil. The decision not to consider harvesting of cutting residues to bioenergy might not always be in line with current forestry practices and could be easily changed to include part of residue carbon into the short-lasting wood products (W_S). While labile storage carbon associated to coarse roots and branches sapwood ($C_S\, B_{\mathrm{OS}}/B_S$) is transferred to CWD, labile storage associated to trunk sapwood ($C_S\, B_{\mathrm{OS}}/B_S$) is split up between WP_L, WP_S analogous to B_{TS}. All carbon in leaves and fine roots (including associated labile storage) and carbon from the transient pool is transferred to the Litter pool.

A.6 MeanTree *state variables and parameters*

Symbol	Unit	Description	Source
r	m	tree radius at trunk base	Section A.3.1
Δr	m	change of tree radius at trunk base	dynamically solved for
r_{BH}	m	radius at breast height	Ogle and Pacala (2009, SI, Eq. (24))
dbh	cm	tree radius at breast height	Section A.3.1
H	m	tree height	Eq. (A.10), Näslund (1947), Siipilehto and Kangas (2015)
GPP	$\mathrm{gC\,yr^{-1}}$	carbon uptake by photosynthesis	-
C_{alloc}	$\mathrm{gC\,yr^{-1}}$	available gC/yr for allocation to tree organs	$E/\Delta t - R_M$
R_M	$\mathrm{gC\,yr^{-1}}$	whole plant maintenance respiration	$M_L + M_R + M_S$
M_L	$\mathrm{gC\,yr^{-1}}$	maintenance respiration leaves	Eq. (A.2)
M_R	$\mathrm{gC\,yr^{-1}}$	maintenance respiration fine roots	analogous to M_L
M_S	$\mathrm{gC\,yr^{-1}}$	maintenance respiration sapwood	Eq. (A.5)
G_L	$\mathrm{gC\,yr^{-1}}$	growth respiration leaves	Eq. (A.3)
G_R	$\mathrm{gC\,yr^{-1}}$	growth respiration fine roots	analogous to G_L
$G_{\mathrm{OS},E}$	$\mathrm{gC\,yr^{-1}}$	growth respiration sapwood from transient carbon	Eq. (A.7)
G_{OS,C_S}	$\mathrm{gC\,yr^{-1}}$	growth respiration sapwood from labile storage carbon	Eq. (A.9)
η_L		CUE during leaf tissue growth	Eq. (A.4)
η_R		CUE during fine root tissue growth	analogous to η_L
η_W		CUE during sapwood production	Eq. (A.8)
η_{HW}		CUE during heartwood production	fixed to 1
H_{TH}	m	height of trunk heartwood section	Ogle and Pacala (2009, SI, Eq. (9)), corrected and introduced capturing of equalities
LA	$\mathrm{m^2}$	total leaf area	SLA B_L
V_T	$\mathrm{m^3}$	trunk volume	Ogle and Pacala (2009, SI, Eq. (9))
V_{TH}	$\mathrm{m^3}$	volume of trunk heartwood section	Ogle and Pacala (2009, SI, Eq. (14)), introduced capturing of equalities
V_{TS}	$\mathrm{m^3}$	volume of trunk sapwood	Ogle and Pacala (2009, SI, Eq. (15))
SW	m	width (or depth) of sapwood at trunk base	Section A.3.5, Helmisaari et al. (2007), Sellin (1994)
C_S^*	$\mathrm{g_{gluc}}$	maximum amount of labile carbon stored in sapwood	Ogle and Pacala (2009, SI, Eq. (5))
B_S^*	$\mathrm{g_{dw}}$	biomass of 'living' sapwood	Ogle and Pacala (2009, SI, Eq. (29))
B_S	gC	biomass of bulk sapwood	$B_{\mathrm{OS}} + B_{\mathrm{TS}}$
δ_S	$\frac{\mathrm{g_{gluc}}}{\mathrm{g_{dw}}}$	concentration of labile carbon storage of bulk sapwood	Eq. (A.23), Ogle and Pacala (2009, SI, Eq. (7))
ρ_W	$\frac{\mathrm{g_{dw}}}{\mathrm{m^3}}$	density of newly produced sapwood	Eq. (A.34)
δ_W	$\frac{\mathrm{g_{gluc}}}{\mathrm{g_{dw}}}$	maximum labile carbon storage capacity of newly produced sapwood	Eq. (A.36), Ogle and Pacala (2009, SI, Eq. (6))
B_T	gC	biomass of trunk	$B_{\mathrm{TH}} + B_{\mathrm{TS}} + \frac{B_{\mathrm{TS}}}{B_S} C_S$
m_X	$\mathrm{g_{dw}}$	allometrically derived biomass of tree organ X	based on Eq. (A.12)
λ_S		ratio of "other" sapwood to trunk sapwood	Eq. (A.39)
λ_H		ratio of "other" heartwood to trunk heartwood	Eq. (A.39)
v_T	$\mathrm{yr^{-1}}$	sapwood to heartwood conversion rate of trunk	Eq. (A.29), Ogle and Pacala (2009, SI, Eq. (2))
v_O	$\mathrm{yr^{-1}}$	sapwood to heartwood conversion rate of coarse roots and branches	Eq. (A.43), Ogle and Pacala (2009, SI, Eq. (1F))
f_L		partitioning from transient pool to leaves	Section A.3.3, Ogle and Pacala (2009, SI, Eq. (1A))
f_R		partitioning from transient pool to fine roots	Section A.3.4, Ogle and Pacala (2009, SI, Eq. (1B))
f_T		partitioning from transient pool to trunk	Section A.3.5, Ogle and Pacala (2009, SI, Eq. (31C))
f_O		partitioning from transient pool to coarse roots and branches	Section A.3.6, Ogle and Pacala (2009, SI, Eq. (1E))
f_{C_S}		fraction of C_S used to regrow "other" sapwood	Eq. (A.44)

Table A.2: Tree module variables. Units are per single tree.

Scots pine

Symbol	Value	Unit	Description	Source
SLA	6.162	$\frac{\mathrm{m}^2}{\mathrm{kg_{dw}}}$	specific leaf area	Goude et al. (2019)
R_{mL}	0.950	$\frac{\mathrm{g_{gluc}}}{\mathrm{g_{dw}}}\ \mathrm{yr}^{-1}$	maintenance respiration rate of leaves	Ogle and Pacala (2009, Table 2)
R_{mR}	0.750	$\frac{\mathrm{g_{gluc}}}{\mathrm{g_{dw}}}\ \mathrm{yr}^{-1}$	maintenance respiration rate of fine roots	Ogle and Pacala (2009, Table 2)
R_{mS}	0.063	$\frac{\mathrm{g_{gluc}}}{\mathrm{g_{dw}}}\ \mathrm{yr}^{-1}$	maintenance respiration rate of sapwood	Lavigne and Ryan (1997, Table 5, northern)
S_L	0.200	yr^{-1}	senescence rate of leaves	Muukkonen (2005, Table 3)
S_R	0.811	yr^{-1}	senescence rate of fine roots	Pukkala (2014, Table 2)
S_O	0.040	yr^{-1}	senescence rate of coarse roots and branches	Vanninen and Mäkelä (2005, Table 1); also following simulations for coarse roots, Eq. (10) leads to 0.06 for branches, we took one of the two
ρ_{RL}	0.670		fine root-to-leaf biomass ratio	Pukkala (2014, Table 2)
η_B	0.045		relative height at which trunk transitions from a neiloid to a paraboloid	Ogle and Pacala (2009, Table 2)
η_C	0.710		relative height at which trunk transitions from a paraboloid to a cone	Ogle and Pacala (2009, Table 2, called η)
γ_X	0.620		xylem conducting area to sapwood area ratio	Ogle and Pacala (2009, Table 2)
γ_C	2.650e+05	$\frac{\mathrm{g_{gluc}}}{\mathrm{m}^3}$	maximum storage capacity of living sapwood cells	Ogle and Pacala (2009, Table 2)
γ_W	6.670e-07	$\frac{\mathrm{m}^3}{\mathrm{g_{dw}}}$	(inverse) density of sapwood structural tissue	Ogle and Pacala (2009, Table 2)
SW_a	18.800		numerator parameter for sapwood width model	Sellin (1994, Eq. 2)
SW_b	60.0		denominator parameter for sapwood width model	Sellin (1994, Eq. 2)
$\mathrm{HW}_{\mathrm{slope}}$	0.480		slope value for heartwood width line	Sellin (1994, Fig. 1)
ρW_{max}	5.500e+05	$\frac{\mathrm{g_{dw}}}{\mathrm{m}^3}$	maximum density of newly produced sapwood	computed to keep δ_W positive
ρW_{min}	2.800e+05	$\frac{\mathrm{g_{dw}}}{\mathrm{m}^3}$	minimum wood density	empirical parameter after some testing
dbh_M	4.0	cm	for dbh $<$ dbh_M the allometrically derived wood density is assumed to be useless	empirical parameter after some testing
δ_L	0.110	$\frac{\mathrm{g_{gluc}}}{\mathrm{g_{dw}}}$	labile carbon storage capacity of leaves	Ogle and Pacala (2009, Table 2)
δ_R	0.080	$\frac{\mathrm{g_{gluc}}}{\mathrm{g_{dw}}}$	labile carbon storage capacity of fine roots	Ogle and Pacala (2009, Table 2)
C_{gL}	2.442	$\frac{\mathrm{g_{gluc}}}{\mathrm{g_{dw}}}$	construction costs of producing leaves	Ryan et al. (1997, p.878) states that leaf construction costs were $28/15 \cdot 0.25$ (of leaf NPP)
C_{gR}	1.597	$\frac{\mathrm{g_{gluc}}}{\mathrm{g_{dw}}}$	construction costs of producing fine roots	Ryan et al. (1997, Table 4) and some empirical adaptation
$C_{g\mathrm{HW}}$	1.0	$\frac{\mathrm{g_{gluc}}}{\mathrm{g_{dw}}}$	construction costs of converting heartwood from labile sapwood (actually: no costs)	missing in Ogle and Pacala (2009) (causing a unit mismatch)
C_{gW}	1.558	$\frac{\mathrm{g_{gluc}}}{\mathrm{g_{dw}}}$	construction costs of producing sapwood	Lavigne and Ryan (1997, Table 5, northern), we add 1.0 because for us growth is not part of the factor to multiply with

Table A.3: Scots pine parameters.

Norway spruce

Symbol	Value	Unit	Description	Source
SLA	5.020	$\frac{\mathrm{m}^2}{\mathrm{kg_{dw}}}$	specific leaf area	Goude et al. (2019)
R_{mL}	0.950	$\frac{\mathrm{g_{gluc}}}{\mathrm{g_{dw}}}\ \mathrm{yr}^{-1}$	maintenance respiration rate of leaves	Ogle and Pacala (2009, Table 2)
R_{mR}	0.750	$\frac{\mathrm{g_{gluc}}}{\mathrm{g_{dw}}}\ \mathrm{yr}^{-1}$	maintenance respiration rate of fine roots	Ogle and Pacala (2009, Table 2)
R_{mS}	0.077	$\frac{\mathrm{g_{gluc}}}{\mathrm{g_{dw}}}\ \mathrm{yr}^{-1}$	maintenance respiration rate of sapwood	Lavigne and Ryan (1997, Table 5, northern)
S_L	0.100	yr^{-1}	senescence rate of leaves	Muukkonen and Lehtonen (2004)
S_R	0.868	yr^{-1}	senescence rate of fine roots	Pukkala (2014, Table 2)
S_O	0.013	yr^{-1}	senescence rate of coarse roots and branches	Muukkonen and Lehtonen (2004)
ρ_{RL}	0.250		fine root-to-leaf biomass ratio	Pukkala (2014, Table 2)
η_B	0.045		relative height at which trunk transitions from a neiloid to a paraboloid	Ogle and Pacala (2009, Table 2) (pine parameter)
η_C	0.710		relative height at which trunk transitions from a paraboloid to a cone	Ogle and Pacala (2009, Table 2, called η) (pine parameter)
γ_X	0.620		xylem conducting area to sapwood area ratio	Ogle and Pacala (2009, Table 2) (pine parameter)
γ_C	2.650e+05	$\frac{\mathrm{g_{gluc}}}{\mathrm{m}^3}$	maximum storage capacity of living sapwood cells	Ogle and Pacala (2009, Table 2) (pine parameter)
γ_W	6.670e-07	$\frac{\mathrm{m}^3}{\mathrm{g_{dw}}}$	(inverse) density of sapwood structural tissue	Ogle and Pacala (2009, Table 2) (pine parameter)
SW_a	18.800		numerator parameter for sapwood width model	Sellin (1994, Eq. 2)
SW_b	60.0		denominator parameter for sapwood width model	Sellin (1994, Eq. 2)
$\mathrm{HW}_{\mathrm{slope}}$	0.480		slope value for heartwood width line	Sellin (1994, Fig. 1)
$\rho_{W_{\mathrm{max}}}$	5.500e+05	$\frac{\mathrm{g_{dw}}}{\mathrm{m}^3}$	maximum density of newly produced sapwood	computed to keep δ_W positive
$\rho_{W_{\mathrm{min}}}$	2.800e+05	$\frac{\mathrm{g_{dw}}}{\mathrm{m}^3}$	minimum wood density	empirical parameter after some testing
dbh_M	4.0	cm	for $\mathrm{dbh} < \mathrm{dbh}_M$ the allometrically derived wood density is assumed to be useless	empirical parameter after some testing
δ_L	0.110	$\frac{\mathrm{g_{gluc}}}{\mathrm{g_{dw}}}$	labile carbon storage capacity of leaves	Ogle and Pacala (2009, Table 2) (pine parameter)
δ_R	0.080	$\frac{\mathrm{g_{gluc}}}{\mathrm{g_{dw}}}$	labile carbon storage capacity of fine roots	Ogle and Pacala (2009, Table 2) (pine parameter)
C_{gL}	2.442	$\frac{\mathrm{g_{gluc}}}{\mathrm{g_{dw}}}$	construction costs of producing leaves	Ryan et al. (1997, p.878) states that leaf construction costs were $28/15 \cdot 0.25$ (of leaf NPP)
C_{gR}	1.601	$\frac{\mathrm{g_{gluc}}}{\mathrm{g_{dw}}}$	construction costs of producing fine roots	Ryan et al. (1997, Table 4) and some empirical adaptation
$C_{g\mathrm{HW}}$	1.0	$\frac{\mathrm{g_{gluc}}}{\mathrm{g_{dw}}}$	construction costs of converting heartwood from labile sapwood (actually: no costs)	missing in Ogle and Pacala (2009) (causing a unit mismatch)
C_{gW}	2.202	$\frac{\mathrm{g_{gluc}}}{\mathrm{g_{dw}}}$	construction costs of producing sapwood	Lavigne and Ryan (1997, Table 5, northern), we add 1.0 because for us growth is not part of the factor to multiply with

Table A.4: Norway spruce parameters.

A.7 Soil module

As described in Section 2.1.3, the soil module describes soil carbon dynamics in a minimalist way, using a three-pool model representing a fast decomposing litter pool (Litter), a slowly decomposing coarse woody debris pool (CWD), and a soil organic carbon pool (SOC) with fixed decomposition and fraction parameters (Table A.5) derived from Hyvönen and Ågren (2001), Peltoniemi et al. (2004) and Koven et al. (2013). A schematic of the soil component is shown in Fig. A.4 and next to it is a description of the associated natural fluxes, not caused by management actions. The turnover rate of Litter is set to $0.43\,\mathrm{yr}^{-1}$ and 50 % of the decomposed carbon is transferred to SOC, while the other 50 % return as heterotrophic respiration to the atmosphere. The CWD pool behaves similarly with a turnover rate equal to $0.056\,\mathrm{yr}^{-1}$ with 50 % transfer to SOC and 50 % respiration. Decomposition of SOC by heterotrophs happens at a rate equal to $0.023\,\mathrm{yr}^{-1}$ in order to match SOC stocks in Peltoniemi et al. (2004, Table 5), and contributes to CO_2 emissions to the atmosphere.

Symbol	**Value**	**Unit**	**Description**	**Source**
k_{Litter}	0.438	yr^{-1}	total Litter turnover rate	Hyvönen and Ågren (2001, Table 2)
f_{Litter}	0.500	yr^{-1}	Litter respiration fraction	Koven et al. (2013, Fig. 2)
k_{CWD}	0.056	yr^{-1}	total CWD turnover rate	Hyvönen and Ågren (2001, Table 2)
f_{CWD}	0.500	yr^{-1}	CWD respiration fraction	Koven et al. (2013, Fig. 2)
k_{SOC}	0.023	yr^{-1}	respiration rate SOC	defined to match SOC stocks in Peltoniemi et al. (2004, Table 5)

Table A.5: Soil module parameters.

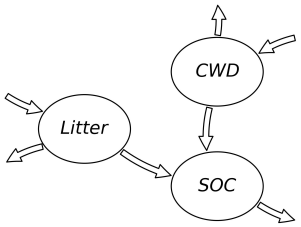

Figure A.4: The soil carbon module.

External output fluxes

- Litter↗: $f_{\text{Litter}} \cdot k_{\text{Litter}} \cdot \text{Litter}$
- CWD↗: $f_{\text{CWD}} \cdot k_{\text{CWD}} \cdot \text{CWD}$
- SOC↗: $k_{\text{SOC}} \cdot \text{SOC}$

Internal fluxes

- $\sum_i S_{L,i} \cdot B_{L,i} + S_{R,i} \cdot B_{R,i} \rightarrow \text{Litter}$
- $\sum_i S_{O,i} \cdot (B_{\text{OS},i} + B_{\text{OH},i}) \rightarrow \text{CWD}$
- Litter $\rightarrow$ SOC: $(1 - f_{\text{Litter}}) \cdot k_{\text{Litter}} \cdot \text{Litter}$
- CWD $\rightarrow$ SOC: $(1 - f_{\text{CWD}}) \cdot k_{\text{CWD}} \cdot \text{CWD}$

Part B Model parameterization and forcing

B.1 Environmental conditions

Climatic conditions refer to those for the years from 2000 to 2019 for Hyytiälä SMEAR II-station (retrieved from avaa-database, located in `data/forcing/FIHy_forcing_1997_2019.dat`, retrieval date 03/11/2020), after removal of the linear trends. The conditions are repeated to cover the whole spinup and simulation periods.

B.2 Carbon dynamics parameters

Parameters for the photosynthesis module, the soil module, and the wood products were taken from literature (Table A.1, Table A.5, Section A.5). The species-specific parameters are listed in Tables A.3 and A.4. When species-specific parameters for spruce were not available, values for pines were used also for spruce (e.g., labile storage capacities of leaves (δ_L) and roots (δ_R), and

the sapwood parameters γ). A small number of species-specific parameters were subject to numerical investigation. Construction costs for producing fine roots were based Ryan et al. (1997, Table 4) and adjusted to make the model match annual radial growth from literature (Repola 2009, Table 3; see Fig. D.1), which is possible because lower root respiration makes more carbon available for trunk growth. Parameters associated to the density of newly grown sapwood ($\rho_{W_{\min}}$, $\rho_{W_{\max}}$, dbh_M) were empirically chosen to keep the overall wood density close to values reported in (Repola, 2006, Fig. 4), while making sure that the maximum labile carbon storage capacity (δ_W) is nonnegative at all times. The ratio of fine roots to leaves biomass (ρ_{RL}) generally depends on soil fertility. The chosen values (Pukkala, 2014, Table 2) were subject to major investigation in order to match annual radial trunk growth (Repola 2009, Table 3; see Fig. D.1) and indicate, at least for pine, a rather low soil fertility (Vanninen and Mäkelä, 2005, Table 1).

Part C Model spinup

Model spinup initializes the stand structure and tree, soil and wood product pools for use in the management scenarios. We used a three-stage spinup to reach reasonable equilibrium pool sizes. First, a uniform pine stand with one *MeanTree* was initiated assuming empty tree, soil and wood-product pools. Initial tree dbh = 1.0 cm and $N = 2000\,\mathrm{ha}^{-1}$. As the *MeanTree* reached a height of 3.0 m a pre-commercial thinning was performed, to reduce N to $1500\,\mathrm{ha}^{-1}$. When the stand basal area (SBA) reached $25\,\mathrm{m}^2\,\mathrm{ha}^{-1}$ the stand was thinned to SBA = $18\,\mathrm{m}^2\,\mathrm{ha}^{-1}$. A clear cut was done after 80 yr, the trees in the stand were replanted and the same simulation ran for another 80 yr. After the second clear cut at 160 yr, the average of photosynthetically derived carbon input, fluxes between the pools, and the pool sizes relative to the last 50 yr were used to compute a pseudo-equilibrium of the carbon stocks in the system (Metzler and Sierra, 2018). These values then served as initial stocks (soil and wood products) for the second identical 160 yr spinup. The subsequent pseudo-equilibrium soil and wood-product stocks were then used as the starting point for the third and last spinup stage, and carbon age distributions were computed from another pseudo-equilibrium based on the last 50 yr. The last spinup stage runs for another 160 yr and starts with four pine *MeanTree*s, each with dbh = 1.0 cm and representing $N_i = 375$ trees per hectare (i.e., a stand density of $N = 1500\,\mathrm{ha}^{-1}$). The first *MeanTree* was cut and replanted after 20 yr and 100 yr, the second one after 40 yr and 120 yr, the third one after 60 yr and 140 yr, and the fourth one after 80 yr. This creates a mixed-aged pine forest, whose carbon stocks are in a reasonable equilibrium with a net carbon balance close to zero ($-0.8\,\mathrm{kgC\,m}^{-2}$), as can be seen from Fig. 3C and Table 2 (INCB, mixed-aged pine, Entire system). The final conditions are used as the common starting point for all management scenarios.

Part D Model benchmarking

For a more in-depth test of the model's biomass predictions, we compare it to the external allometric functions based on dbh. The statistical allometric relationships for the biomasses of tree organs depend on one single dbh value. The different presented management scenarios, however, consist of differently sized *MeanTree*s with the external allometric relations applied to each of them separately. Consequently, we ran two ad hoc single-species (pine, spruce) simulations with a single *MeanTree* each, comparing the tree organs' biomasses from the two simulations with its associated external statistical allometries. In this way we guarantee that leaf biomass follows perfectly the observations (Fig. D.2A), which is expected because the *MeanTree*'s leaf biomass is directly defined by the allometric equation depending on its diameter at breast height. Fine root biomass is perfectly defined by a fixed fine root-to-leaf biomass ratio (ρ_{RL}). We test discrepancies in the modelled and observed biomasses of other organs.

The density of newly produced sapwood is dynamically adapted in the model in order to follow the predicted trunk wood biomass, and we can see a perfect match Fig. D.2B. Because the biomass of coarse roots and living branches is linked to trunk biomass via a dynamic factor λ (Eq. A.39), this perfect match carries over to the biomass of living branches and coarse roots ("other", Fig. D.2C) and in turn to total tree biomass (Fig. D.2D, without fine roots).

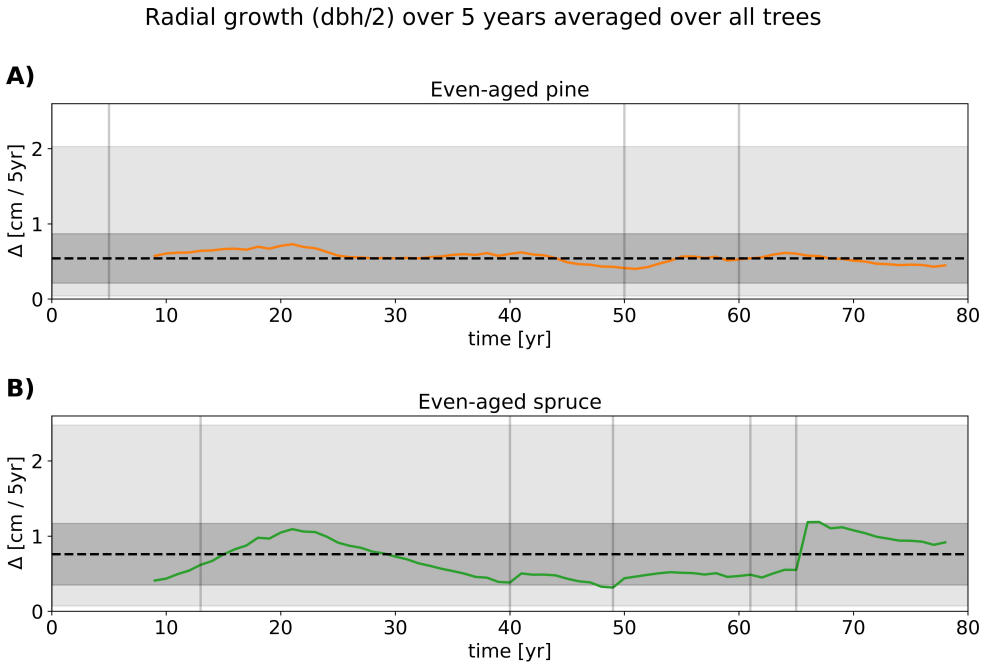

Figure D.1: Radial growth of the two even-aged single-species scenarios. The dark solid graph indicates the radial growth (Δ dbh/2) over the last five years, averaged over all trees in the stand according to the respective management scenario. The dashed horizontal line marks the mean value, the dark gray area the standard deviation around the mean, and the light gray area the range between the minimum and maximum values of the stand inventory data described in Repola (2009, Table 3).

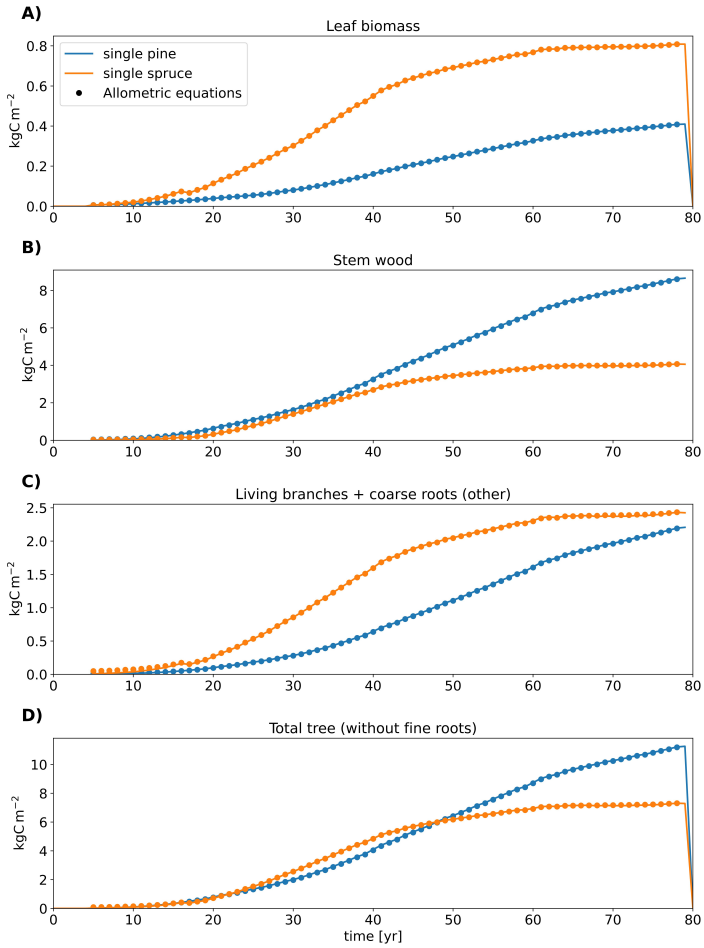

Figure D.2: Model accuracy with respect to external allometries. Different tree organs' carbon content over time (solid lines) and their statistical counterparts as derived from Repola and Ahnlund Ulvcrona (2014), Repola (2009) and Lehtonen (2005) (dots), based on the diameter at breast height of the single-tree simulations for benchmarking.

Part E Supplementary figures

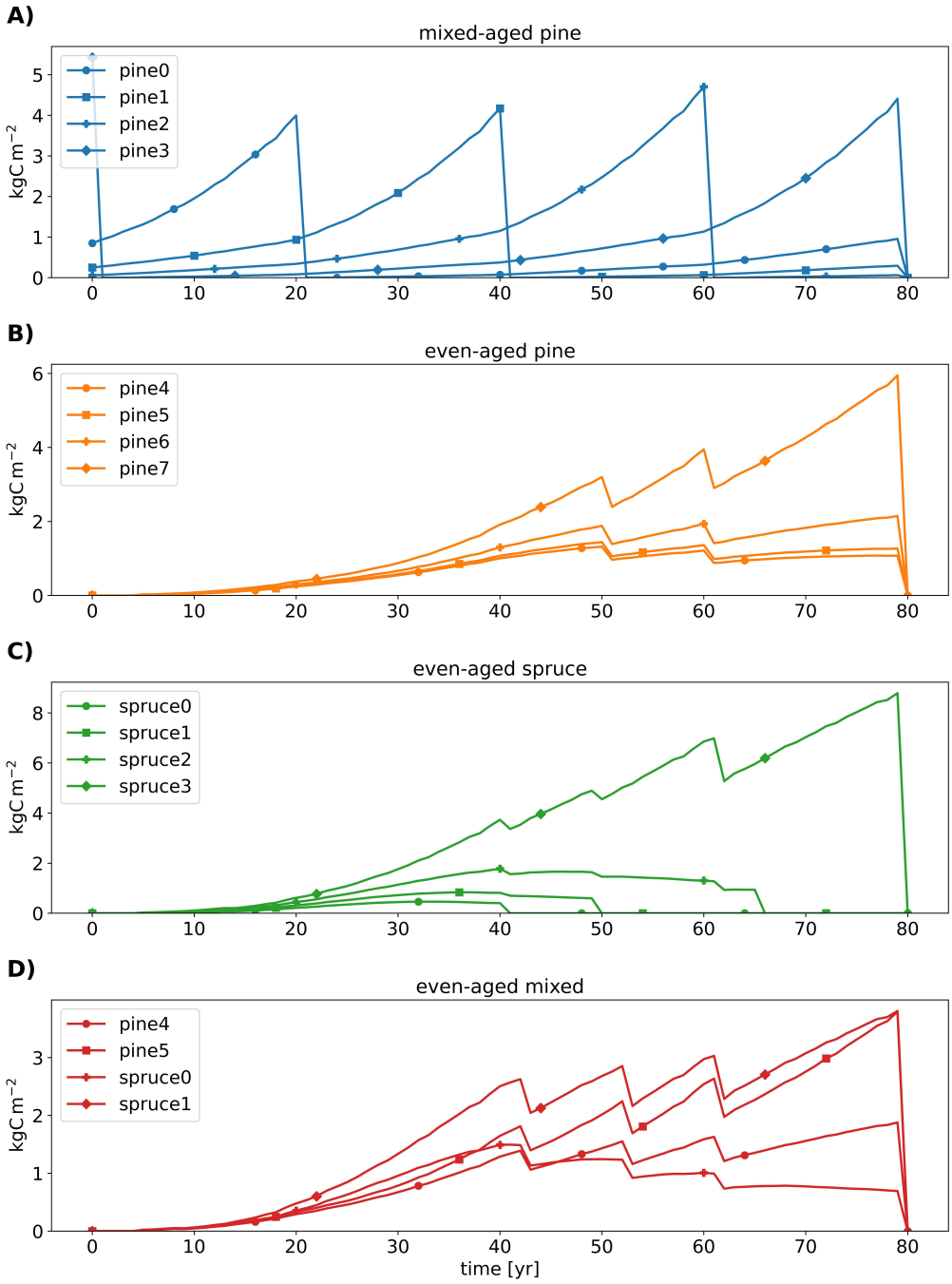

Figure E.1: Time series of carbon in *MeanTrees*. Different panels show different management scenarios.

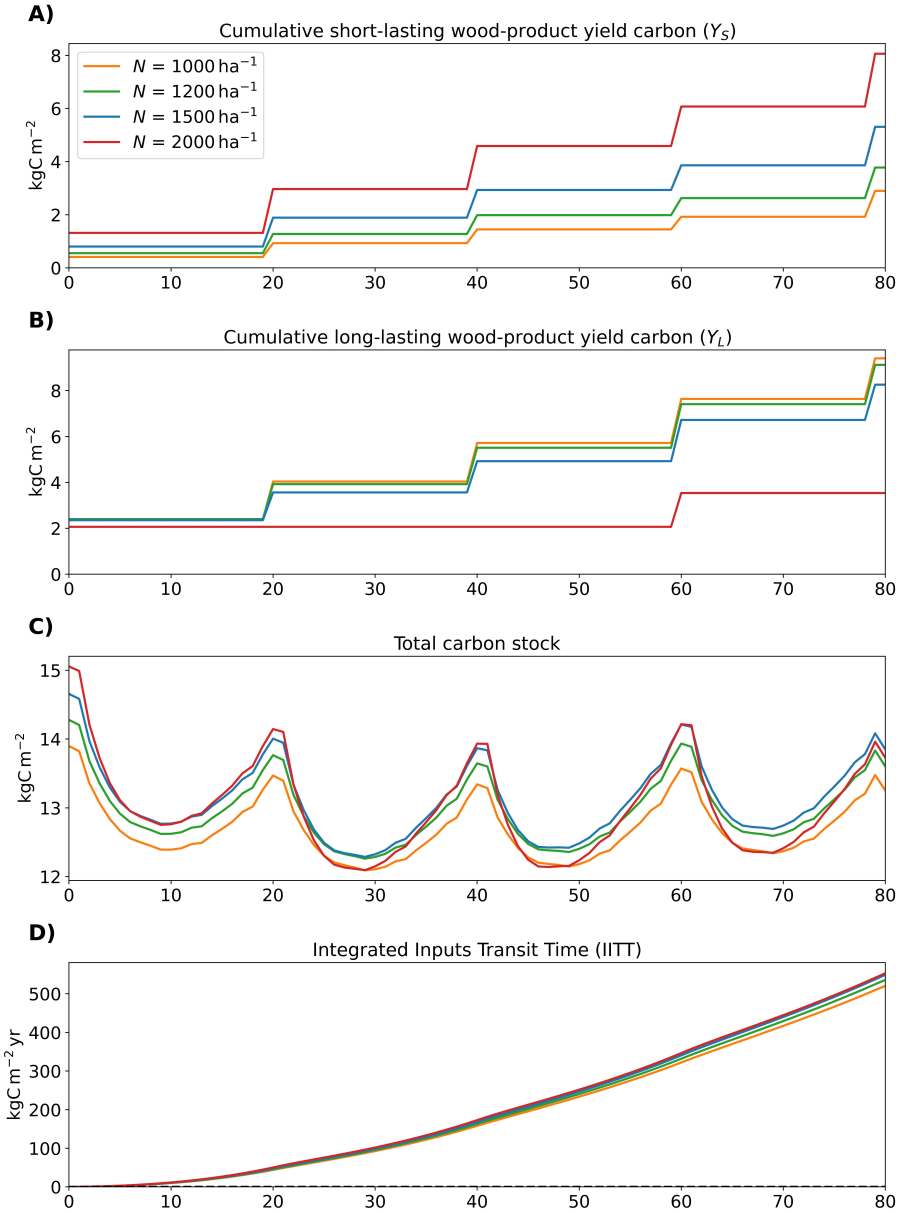

Figure E.2: Temporal evolution of short-lasting and long-lasting wood production, carbon sequestration and climate change mitigation potential metrics for mixed-aged pine scenarios with different tree densities (N). A) Cumulative short-lasting wood-product yield carbon (Y_S, Eq. (5)). B) Cumulative long-lasting wood-product yield carbon (Y_S, Eq. (5)). C) Total carbon stock including trees, soil, and wood products. D) Integrated Inputs Transit Time (IITT, Eq. (8)).

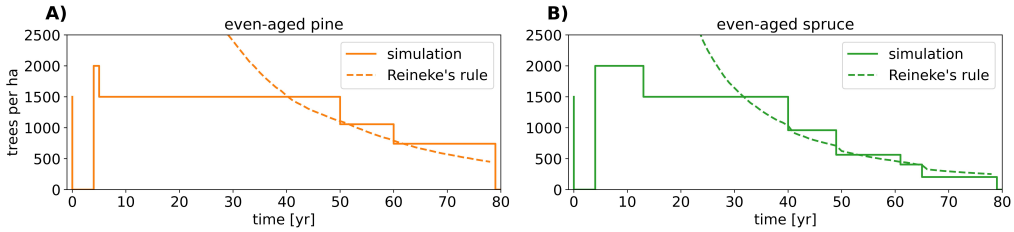

Figure E.3: Reineke's rule self-thinning rule (dashed lines) and the thinning in different management scenarios (solid lines). A) even-aged pine, B) even-aged spruce.

References

Evy Ampoorter, Luc Barbaro, Hervé Jactel, Lander Baeten, Johanna Boberg, Monique Carnol, Bastien Castagneyrol, Yohan Charbonnier, Seid Muhie Dawud, Marc Deconchat, et al. Tree diversity is key for promoting the diversity and abundance of forest-associated taxa in Europe. *Oikos*, 129(2):133–146, 2020.

David H Anderson. *Compartmental modeling and tracer kinetics*, volume 50. Springer Science & Business Media, 1983.

Rasmus Astrup, Pierre Y Bernier, Hélène Genet, David A Lutz, and Ryan M Bright. A sensible climate solution for the boreal forest. *Nature Climate Change*, 8(1):11–12, 2018.

Dennis Baldocchi, Francis M Kelliher, T Aet Black, and Paul Jarvis. Climate and vegetation controls on boreal zone energy exchange. *Global Change Biology*, 6(S1):69–83, 2000.

Jürgen Bauhus, David I Forrester, Barry Gardiner, Hervé Jactel, Ramon Vallejo, and Hans Pretzsch. Ecological stability of mixed-species forests. In *Mixed-species forests*, pages 337–382. Springer, 2017.

Yves Bergeron, Mike Flannigan, Sylvie Gauthier, Alain Leduc, and Patrick Lefort. Past, current and future fire frequency in the Canadian boreal forest: implications for sustainable forest management. *Ambio*, 33(6):356–360, 2004.

Dan Berggren Kleja, Magnus Svensson, Hooshang Majdi, Per-Erik Jansson, Ola Langvall, Bo Bergkvist, Maj-Britt Johansson, Per Weslien, Laimi Truusb, Anders Lindroth, and Göran I Ågren. Pools and fluxes of carbon in three Norway spruce stands along a climatic gradient in Sweden. *Biogeochemistry*, 2007.

Bert Bolin and Henning Rodhe. A note on the concepts of age distribution and transit time in natural reservoirs. *Tellus*, 25(1):58–62, 1973.

Gordon B Bonan. Forests and climate change: forcings, feedbacks, and the climate benefits of forests. *Science*, 320(5882):1444–1449, 2008.

Pål Börjesson, Julia Hansson, and Göran Berndes. Future demand for forest-based biomass for energy purposes in Sweden. *Forest Ecology and Management*, 383:17–26, 2017.

Roger W Brockett. *Finite Dimensional Linear Systems*, volume 74. SIAM, 2015.

Harald Bugmann. A review of forest gap models. *Climatic Change*, 51(3): 259–305, 2001.

Richard T Busing and Daniel Mailly. Advances in spatial, individual-based modelling of forest dynamics. *Journal of Vegetation Science*, 15(6):831–842, 2004.

MGR Cannell and RC Dewar. Carbon allocation in trees: a review of concepts for modelling. *Advances in ecological research*, 25:59–104, 1994.

Mariah S Carbone, Claudia I Czimczik, Kelsey E McDuffee, and Susan E Trumbore. Allocation and residence time of photosynthetic products in a boreal forest using a low-level ^{14}C pulse-chase labeling technique. *Global Change Biology*, 13(2):466–477, 2007.

Mariah S Carbone, Claudia I Czimczik, Trevor F Keenan, Paula F Murakami, Neil Pederson, Paul G Schaberg, Xiaomei Xu, and Andrew D Richardson. Age, allocation and availability of nonstructural carbon in mature red maple trees. *New Phytologist*, 200(4):1145–1155, 2013.

FS Chapin III, AD McGuire, J Randerson, R Pielke, Dennis Baldocchi, SE Hobbie, Nigel Roulet, W Eugster, E Kasischke, EB Rastetter, et al.

Arctic and boreal ecosystems of western North America as components of the climate system. *Global Change Biology*, 6(S1):211–223, 2000.

G D Farquhar, S V Caemmerer, and J A Berry. A biochemical model for photosynthetic CO_2 assimilation in leaves of C_3 species. *Planta*, 149(1): 78–90, 1980.

Michael Fell and Kiona Ogle. Refinement of a theoretical trait space for North American trees via environmental filtering. *Ecological Monographs*, 88(3):372–384, 2018.

Michael Fell, Jarrett Barber, Jeremy W Lichstein, and Kiona Ogle. Multidimensional trait space informed by a mechanistic model of tree growth and carbon allocation. *Ecosphere*, 9(1):e02060, 2018.

Terje Gobakken, Nils L Lexerød, and Tron Eid. T: A forest simulator for bioeconomic analyses based on models for individual trees. *Scandinavian Journal of Forest Research*, 23(3):250–265, 2008.

Martin Goude, Urban Nilsson, and Emma Holmström. Comparing direct and indirect leaf area measurements for Scots pine and Norway spruce plantations in Sweden. *European Journal of Forest Research*, 138(6):1033–1047, 2019.

Andrei Gromtsev. Natural disturbance dynamics in the boreal forests of European Russia: a review. *Silva Fennica*, 36(1):41–55, 2002.

Vegard Sverre Gundersen and Lars Helge Frivold. Public preferences for forest structures: A review of quantitative surveys from Finland, Norway and Sweden. *Urban Forestry & Urban Greening*, 7(4):241–258, 2008.

Corinna Hawkes. Woody plant mortality algorithms: description, problems and progress. *Ecological Modelling*, 126(2-3):225–248, 2000.

Heljä-Sisko Helmisaari, John Derome, Pekka Nöjd, and Mikko Kukkola. Fine root biomass in relation to site and stand characteristics in Norway spruce and Scots pine stands. *Tree Physiology*, 27(10):1493–1504, 2007.

P Högberg, LA Ceder, R Astrup, D Binkley, L Dalsgaard, G Egnell, A Filipchuk, H Genet, A Ilintsev, WA Kurz, et al. Sustainable boreal forest management challenges and opportunities for climate change mitigation. 2021.

Emma Holmström, Martin Goude, Oscar Nilsson, Annika Nordin, Tomas Lundmark, and Urban Nilsson. Productivity of Scots pine and Norway spruce in central Sweden and competitive release in mixtures of the two species. *Forest Ecology and Management*, 429:287–293, 2018.

Riku Huttunen, Petteri Kuuva, Markku Kinnunen, Bettina Lemström, and Petri Hirvonen. Carbon neutral Finland 2035 - national climate and energy strategy. 2022.

Saija Huuskonen, Timo Domisch, Leena Finér, Jarkko Hantula, Jari Hynynen, Juho Matala, Jari Miina, Seppo Neuvonen, Seppo Nevalainen, Pentti Niemistö, et al. What is the potential for replacing monocultures with mixed-species stands to enhance ecosystem services in boreal forests in Fennoscandia? *Forest ecology and management*, 479:118558, 2021.

Jari Hynynen, Risto Ojansuu, Hannu Hökkä, Jouni Siipilehto, Hannu Salminen, and Pekka Haapala. *Models for predicting stand development in MELA system*. Metsäntutkimuslaitos, 2002.

Riitta Hyvönen and Göran I Ågren. Decomposer invasion rate, decomposer growth rate, and substrate chemical quality: how they influence soil organic matter turnover. *Canadian Journal of Forest Research*, 31(9):1594–1601, 2001.

John A Jacquez and Carl P Simon. Qualitative theory of compartmental systems. *Siam Review*, 35(1):43–79, 1993.

Hervé Jactel, Xoaquín Moreira, and Bastien Castagneyrol. Tree diversity and forest resistance to insect pests: patterns, mechanisms, and prospects. *Annual Review of Entomology*, 66:277–296, 2021.

Robert Jandl, Marcus Lindner, Lars Vesterdal, Bram Bauwens, Rainer Baritz, Frank Hagedorn, Dale W Johnson, Kari Minkkinen, and Kenneth A Byrne. How strongly can forest management influence soil carbon sequestration? *Geoderma*, 137(3-4):253–268, 2007a.

Robert Jandl, Lars Vesterdal, Mats Olsson, Oliver Bens, Franz Badeck, and J Roc. Carbon sequestration and forest management. *CABI Reviews*, (2007):16–pp, 2007b.

DS Jenkinson and JH Rayner. The turnover of soil organic matter in some of the Rothamsted classical experiments. *Soil science*, 123(5):298–305, 1977.

Jens Kattge and Wolfgang Knorr. Temperature acclimation in a biochemical model of photosynthesis: a reanalysis of data from 36 species. *Plant, cell & environment*, 30(9):1176–1190, 2007.

Seppo Kellomäki. *Management of Boreal Forests: Theories and Applications for Ecosystem Services*. Springer Nature, 2022.

Seppo Kellomäki, Heli Peltola, Tuula Nuutinen, Kari T Korhonen, and Harri Strandman. Sensitivity of managed boreal forests in Finland to climate change, with implications for adaptive management. *Philosophical Transactions of the Royal Society B: Biological Sciences*, 363(1501):2339–2349, 2008.

Pasi Kolari, Hanna K Lappalainen, Heikki HäNninen, and Pertti Hari. Relationship between temperature and the seasonal course of photosynthesis

in Scots pine at northern timberline and in southern boreal zone. *Tellus B: Chemical and Physical Meteorology*, 59(3):542–552, 2007.

Taneli Kolström. Modelling the development of an uneven-aged stand of Picea abies. *Scandinavian Journal of Forest Research*, 8(1-4):373–383, 1993.

CD Koven, WJ Riley, ZM Subin, JY Tang, MS Torn, WD Collins, GB Bonan, DM Lawrence, and SC Swenson. The effect of vertically resolved soil biogeochemistry and alternate soil C and N models on C dynamics of CLM4. *Biogeosciences*, 10(11):7109–7131, 2013.

Timo Kuuluvainen, Tuomas Aakala, et al. Natural forest dynamics in boreal Fennoscandia: a review and classification. *Silva Fennica*, 45(5):823–841, 2011.

Timo Kuuluvainen, Olli Tahvonen, and Tuomas Aakala. Even-aged and uneven-aged forest management in boreal Fennoscandia: a review. *Ambio*, 41(7):720–737, 2012.

Jouko Laasasenaho. *Taper curve and volume functions for pine, spruce and birch*. Metsäntutkimuslaitos, 1982.

André Lacointe. Carbon allocation among tree organs: a review of basic processes and representation in functional-structural tree models. *Annals of Forest Science*, 57(5):521–533, 2000.

Erkki Lähde, Olavi Laiho, and C Julian Lin. Silvicultural alternatives in an uneven-sized forest dominated by Picea abies. *Journal of forest research*, 15(1):14–20, 2010.

JJ Landsberg and RH Waring. A generalised model of forest productivity using simplified concepts of radiation-use efficiency, carbon balance and partitioning. *Forest ecology and management*, 95(3):209–228, 1997.

Jørgen Bo Larsen, Per Angelstam, Jürgen Bauhus, João Fidalgo Carvalho, Jurij Diaci, Dorota Dobrowolska, Anna Gazda, Lena Gustafsson, Frank Krumm, Thomas Knoke, et al. *Closer-to-Nature Forest Management. From Science to Policy 12.*, volume 12. EFI European Forest Institute, 2022.

Samuli Launiainen, Gabriel G Katul, Ari Lauren, and Pasi Kolari. Coupling boreal forest CO_2, H_2O and energy flows by a vertically structured forest canopy – soil model with separate bryophyte layer. *Ecological Modelling*, 312:385–405, 2015.

Samuli Launiainen, Gabriel G Katul, Pasi Kolari, Anders Lindroth, Annalea Lohila, Mika Aurela, Andrej Varlagin, Achim Grelle, and Timo Vesala. Do the energy fluxes and surface conductance of boreal coniferous forests in Europe scale with leaf area? *Global Change Biology*, 22(12):4096–4113, 2016.

Samuli Launiainen, Mingfu Guan, Aura Salmivaara, and Antti-Jussi Kieloaho. Modeling boreal forest evapotranspiration and water balance at stand and catchment scales: a spatial approach. *Hydrology and Earth System Sciences*, 23(8):3457–3480, 2019.

Samuli Launiainen, Gabriel G Katul, Kersti Leppä, Pasi Kolari, Toprak Aslan, Tiia Grönholm, Lauri Korhonen, Ivan Mammarella, and Vesala Timo. Does increasing atmospheric CO_2 explain increasing carbon sink of a boreal coniferous forest? *Global Change Biology*, 2022.

MB Lavigne and MG Ryan. Growth and maintenance respiration rates of aspen, black spruce and jack pine stems at northern and southern BOREAS sites. *Tree Physiology*, 17(8-9):543–551, 1997.

Xavier Le Roux, André Lacointe, Abraham Escobar-Gutiérrez, and Séverine Le Dizès. Carbon-based models of individual tree growth: a critical appraisal. *Annals of Forest Science*, 58(5):469–506, 2001.

Aleksi Lehtonen. Estimating foliage biomass in Scots pine (Pinus sylvestris) and Norway spruce (Picea abies) plots. *Tree Physiology*, 25(7):803–811, 2005.

Timothy M Lenton, Hermann Held, Elmar Kriegler, Jim W Hall, Wolfgang Lucht, Stefan Rahmstorf, and Hans Joachim Schellnhuber. Tipping elements in the Earth's climate system. *Proceedings of the national Academy of Sciences*, 105(6):1786–1793, 2008.

Kersti Leppä, Mika Korkiakoski, Mika Nieminen, Raija Laiho, Juha-Pekka Hotanen, Antti-Jussi Kieloaho, Leila Korpela, Tuomas Laurila, Annalea Lohila, Kari Minkkinen, Raisa Mäkipää, Paavo Ojanen, Meeri Pearson, Timo Penttilä, Juha-Pekka Tuovinen, and Samuli Launiainen. Vegetation controls of water and energy balance of a drained peatland forest: Responses to alternative harvesting practices. *Agricultural and Forest Meteorology*, 295:108198, 2020.

Jari Liski, Ari Pussinen, Kim Pingoud, Raisa Mäkipää, and Timo Karjalainen. Which rotation length is favourable to carbon sequestration? *Canadian Journal of Forest Research*, 31(11):2004–2013, 2001.

Michel Loreau. Biodiversity and ecosystem stability: New theoretical insights. *The Ecological and Societal Consequences of Biodiversity Loss*, pages 145–166, 2022.

Yiqi Luo and Ensheng Weng. Dynamic disequilibrium of the terrestrial carbon cycle under global change. *Trends in Ecology & Evolution*, 26(2): 96–104, 2011.

Sebastiaan Luyssaert, E Schulze, Annett Börner, Alexander Knohl, Dominik Hessenmöller, Beverly E Law, Philippe Ciais, John Grace, et al. Old-growth forests as global carbon sinks. *Nature*, 455(7210):213–215, 2008.

Joachim Maes, Camino Liquete, Anne Teller, Markus Erhard, Maria Luisa Paracchini, José I Barredo, Bruna Grizzetti, Ana Cardoso, Francesca Somma, Jan-Erik Petersen, et al. An indicator framework for assessing ecosystem services in support of the EU Biodiversity Strategy to 2020. *Ecosystem services*, 17:14–23, 2016.

Annikki Mäkelä. A carbon balance model of growth and self-pruning in trees based on structural relationships. *Forest Science*, 43(1):7–24, 1997.

Stefano Manzoni and Amilcare Porporato. Soil carbon and nitrogen mineralization: Theory and models across scales. *Soil Biology and Biochemistry*, 41(7):1355–1379, 2009.

Ole Martin Bollandsås, Joseph Buongiorno, and Terje Gobakken. Predicting the growth of stands of trees of mixed species and size: A matrix model for Norway. *Scandinavian Journal of Forest Research*, 23(2):167–178, 2008.

BE Medlyn, Erwin Dreyer, D Ellsworth, M Forstreuter, PC Harley, MUF Kirschbaum, Xavier Le Roux, Pierre Montpied, J Strassemeyer, A Walcroft, et al. Temperature response of parameters of a biochemically based model of photosynthesis. II. a review of experimental data. *Plant, Cell & Environment*, 25(9):1167–1179, 2002.

Belinda E. Medlyn, Remko A. Duursma, Derek Eamus, David S. Ellsworth, I. Colin Prentice, Craig V. M. Barton, Kristine Y. Crous, Paolo De Angelis, Michael Freeman, and Lisa Wingate. Reconciling the optimal and empirical approaches to modelling stomatal conductance. *Global Change Biology*, 18 (11):3476–3476, 2012.

Christian Messier, Jürgen Bauhus, Rita Sousa-Silva, Harald Auge, Lander Baeten, Nadia Barsoum, Helge Bruelheide, Benjamin Caldwell, Jeannine Cavender-Bares, Els Dhiedt, et al. For the sake of resilience and multifunctionality, let's diversify planted forests! *Conservation Letters*, 15(1): e12829, 2022.

Holger Metzler and Carlos A Sierra. Linear autonomous compartmental models as continuous-time Markov chains: Transit-time and age distributions. *Mathematical Geosciences*, 50(1):1–34, 2018.

Holger Metzler, Markus Müller, and Carlos A Sierra. Transit-time and age distributions for nonlinear time-dependent compartmental systems. *Proceedings of the National Academy of Sciences*, 115:201705296, 01 2018. doi: 10.1073/pnas.1705296115.

Holger Metzler, Qing Zhu, William Riley, Alison Hoyt, Markus Müller, and Carlos A Sierra. Mathematical reconstruction of land carbon models from their numerical output: Computing soil radiocarbon from ^{12}C dynamics. *Journal of Advances in Modeling Earth Systems*, 12(1), 2020.

P Mikola. Selection forestry. *Silva Fennica*, 18:293–301, 1984.

MEA Millennium ecosystem assessment. *Ecosystems and human well-being*, volume 5. Island press Washington, DC, 2005.

Jan Muhr, Alon Angert, Robinson I Negrón-Juárez, Waldemar Alegria Muñoz, Guido Kraemer, Jeffrey Q Chambers, and Susan E Trumbore. Carbon dioxide emitted from live stems of tropical trees is several years old. *Tree Physiology*, 33(7):743–752, 2013.

Petteri Muukkonen. Needle biomass turnover rates of Scots pine (Pinus sylvestris L.) derived from the needle-shed dynamics. *Trees*, 19(3):273–279, 2005.

Petteri Muukkonen and Aleksi Lehtonen. Needle and branch biomass turnover rates of Norway spruce (Picea abies). *Canadian Journal of Forest Research*, 34(12):2517–2527, 2004.

Manfred Näslund. Skogsförsöksanstaltens gallringsförsök i tallskog. 1936.

Manfred Näslund. Funktioner och tabeller för kubering av stående träd. 36 (3):1–81, 1947.

Asko Noormets, Daniel Epron, Jean-Christophe Domec, SG McNulty, T Fox, G Sun, and JS King. Effects of forest management on productivity and carbon sequestration: A review and hypothesis. *Forest Ecology and Management*, 355:124–140, 2015.

Kiona Ogle and Stephen W Pacala. A modeling framework for inferring tree growth and allocation from physiological, morphological and allometric traits. *Tree Physiology*, 29(4):587–605, 2009.

Stephen W Pacala, Charles D Canham, John Saponara, John A Silander Jr, Richard K Kobe, and Eric Ribbens. Forest models defined by field measurements: estimation, error analysis and dynamics. *Ecological monographs*, 66(1):1–43, 1996.

Yude Pan, Richard A Birdsey, Jingyun Fang, Richard Houghton, Pekka E Kauppi, Werner A Kurz, Oliver L Phillips, Anatoly Shvidenko, Simon L Lewis, Josep G Canadell, et al. A large and persistent carbon sink in the world's forests. *Science*, 333(6045):988–993, 2011.

William J Parton, David S Schimel, C Vernon Cole, and Dennis S Ojima. Analysis of factors controlling soil organic matter levels in Great Plains grasslands. *Soil Science Society of America Journal*, 51(5):1173–1179, 1987.

Mikko Peltoniemi, Raisa Mäkipää, Jari Liski, and Pekka Tamminen. Changes in soil carbon with stand age–an evaluation of a modelling method with empirical data. *Global Change Biology*, 10(12):2078–2091, 2004.

Tähti Pohjanmies, María Triviño, Eric Le Tortorec, Adriano Mazziotta, Tord Snäll, and Mikko Mönkkönen. Impacts of forestry on boreal forests: An ecosystem services perspective. *Ambio*, 46(7):743–755, 2017.

Timo Pukkala. Does biofuel harvesting and continuous cover management increase carbon sequestration? *Forest Policy and Economics*, 43:41–50, 2014.

Timo Pukkala. Calculating the additional carbon sequestration of Finnish forestry. *Journal of Sustainable Forestry*, pages 1–18, 2020.

Timo Pukkala, Erkki Lähde, and Olavi Laiho. Growth and yield models for uneven-sized forest stands in Finland. *Forest Ecology and Management*, 258(3):207–216, 2009.

Göran I Ågren and J Fredrik Wikström. Modelling carbon allocation — a review. *NZJ For. Sci*, 23:343–353, 1993.

Martin Rasmussen, Alan Hastings, Matthew J. Smith, Folashade B. Agusto, Benito M. Chen-Charpentier, Forrest M. Hoffman, Jiang Jiang, Katherine E. O. Todd-Brown, Ying Wang, Ying-Ping Wang, and Yiqi Luo. Transit times and mean ages for nonautonomous and autonomous compartmental systems. *Journal of Mathematical Biology*, 73(6-7):1379–1398, apr 2016. doi: 10.1007/s00285-016-0990-8.

Lester Henry Reineke. Perfection a stand-density index for even-aged forest. *Journal of Agricultural Research*, 46:627–638, 1933.

Jaakko Repola. Models for vertical wood density of Scots pine, Norway spruce and birch stems, and their application to determine average wood density. 2006.

Jaakko Repola. Biomass equations for Scots pine and Norway spruce in Finland. 2009.

Jaakko Repola and Kristina Ahnlund Ulvcrona. Modelling biomass of young and dense Scots pine (Pinus sylvestris L.) dominated mixed forests in northern Sweden. 2014.

Robert G Ribe. The aesthetics of forestry: what has empirical preference research taught us? *Environmental management*, 13(1):55–74, 1989.

José Riofrío, Miren del Río, Douglas A Maguire, and Felipe Bravo. Species mixing effects on height–diameter and basal area increment models for Scots pine and Maritime pine. *Forests*, 10(3):249, 2019.

Ricardo Ruiz-Peinado, Hans Pretzsch, Magnus Löf, Michael Heym, Kamil Bielak, Jorge Aldea, Ignacio Barbeito, Gediminas Brazaitis, Lars Drössler, Kšištof Godvod, Aksel Granhus, Stig-Olof Holm, Aris Jansons, Ekaterina Makrickienė, Marek Metslaid, Sandra Metslaid, Arne Nothdurft, Ditlev Otto Juel Reventlow, Roman Sitko, Gintarė Stankevičienė, and Miren del Río. Mixing effects on Scots pine (Pinus sylvestris L.) and Norway spruce (Picea abies L. Karst.) productivity along a climatic gradient across Europe. *Forest Ecology and Management*, 482:118834, 2021. ISSN 0378-1127. doi: https://doi.org/10.1016/j.foreco.2020.118834. URL `https://www.sciencedirect.com/science/article/pii/S0378112720316030`.

Michael G Ryan, Michael B Lavigne, and Stith T Gower. Annual carbon cost of autotrophic respiration in boreal forest ecosystems in relation to species and climate. *Journal of Geophysical Research: Atmospheres*, 102 (D24):28871–28883, 1997.

Ernst Detlef Schulze, Carlos A Sierra, Vincent Egenolf, Rene Woerdehoff, Roland Irslinger, Conrad Baldamus, Inge Stupak, and Hermann Spellmann. The climate change mitigation effect of bioenergy from sustainably managed forests in Central Europe. *GCB Bioenergy*, 12(3):186–197, 2020.

Arne Sellin. Sapwood–heartwood proportion related to tree diameter, age, and growth rate in Picea abies. *Canadian Journal of Forest Research*, 24 (5):1022–1028, 1994.

KP Shine, RG Derwent, DJ Wuebbles, and JJ Morcrette. Radiative forcing of climate in climate change: The IPCC scientific assessment, report prepared

for the Intergovernmental Panel on Climate Change by working group 1, 1990.

Ekaterina Shorohova, Timo Kuuluvainen, Ahto Kangur, and Kalev Jõgiste. Natural stand structures, disturbance regimes and successional dynamics in the Eurasian boreal forests: a review with special reference to Russian studies. *Annals of Forest Science*, 66(2):1–20, 2009.

Carlos A Sierra and Markus Müller. A general mathematical framework for representing soil organic matter dynamics. *Ecological Monographs*, 85(4): 505–524, 2015. doi: 10.1890/15-0361.1.

Carlos A Sierra, Markus Müller, Holger Metzler, Stefano Manzoni, and Susan E Trumbore. The muddle of ages, turnover, transit, and residence times in the carbon cycle. *Global Change Biology*, 23(5):1763–1773, 2017.

Carlos A Sierra, Verónika Ceballos-Núñez, Holger Metzler, and Markus Müller. Representing and understanding the carbon cycle using the theory of compartmental dynamical systems. *Journal of Advances in Modeling Earth Systems*, 2018. doi: 10.1029/2018MS001360.

Carlos A Sierra, Susan E Crow, Martin Heimann, Holger Metzler, Ernst-Detlef Schulze, et al. The climate benefit of carbon sequestration. *Biogeosciences*, 2021.

Carlos A Sierra, V Ceballos-Núñez, . Hartmann, D Herrera-Ramírez, and H Metzler. Ideas and perspectives: Allocation of carbon from net primary production in models is inconsistent with observations of the age of respired carbon. *EGUsphere*, 2022:1–19, 2022. doi: 10.5194/egusphere-2022-34. URL `https://egusphere.copernicus.org/preprints/egusphere-2022-34/`.

Jouni Siipilehto. A comparison of two parameter prediction methods for stand structure in Finland. 2000.

Jouni Siipilehto and Annika Kangas. Näslundin pituuskäyrä ja siihen perustuvia malleja läpimitan ja pituuden välisestä riippuvuudesta suomalaisissa talousmetsissä. 2015.

Frank F Sterck, Marleen AE Vos, S Emilia SE Hannula, Steven SPC de Goede, Wim W de Vries, Jan J den Ouden, Gert-Jan GJ Nabuurs, Wim WH van der Putten, and Ciska GF Veen. Optimizing stand density for climate-smart forestry: A way forward towards resilient forests with enhanced carbon storage under extreme climate events. *Soil Biology and Biochemistry*, 162:108396, 2021.

Timo Tahvanainen and Eero Forss. Individual tree models for the crown biomass distribution of Scots pine, Norway spruce and birch in Finland. *Forest ecology and management*, 255(3-4):455–467, 2008.

María Triviño, Alejandra Morán-Ordoñez, Kyle Eyvindson, Clemens Blattert, Daniel Burgas, Anna Repo, Tähti Pohjanmies, Lluís Brotons, Tord Snäll, and Mikko Mönkkönen. Future supply of boreal forest ecosystem services is driven by management rather than by climate change. *Global Change Biology*, 29(6):1484–1500, 2023.

M Th Van Genuchten. A closed-form equation for predicting the hydraulic conductivity of unsaturated soils. *Soil science society of America journal*, 44(5):892–898, 1980.

Heidi Vanhanen, Ragnar Jonsson, Yuri Gerasimov, Olga Krankina, Christian Messieur, et al. Making boreal forests work for people and nature. 2012.

Petteri Vanninen and Annikki Mäkelä. Carbon budget for Scots pine trees: effects of size, competition and site fertility on growth allocation and production. *Tree Physiology*, 25(1):17–30, 2005.

Petteri Vihervaara, Timo Kumpula, Ari Tanskanen, and Benjamin Burkhard. Ecosystem services–A tool for sustainable management of human–

environment systems. Case study Finnish Forest Lapland. *Ecological complexity*, 7(3):410–420, 2010.

Tiia Yrjölä. *Forest management guidelines and practices in Finland, Sweden and Norway.* European Forest Institute, 2002.

W. G. Zhao and R. J. Qualls. A multiple-layer canopy scattering model to simulate shortwave radiation distribution within a homogeneous plant canopy. *Water Resources Research*, 41(8):A08409, 2005.